S. Sritharan, S. Pampanin, J. Conley

Design Verification, Instrumentation & Test Procedures

PRESSS-3: THE FIVE-STORY PRECAST TEST BUILDING, VOL. 3-3

Final

REPORT

IOWA STATE UNIVERSITY
OF SCIENCE AND TECHNOLOGY

Department of Civil and Construction Engineering
Soil-Structure-Materials Research Group

PRECAST SEISMIC STRUCTURAL SYSTEMS

Design Verification, Instrumentation & Test Procedures

PRESSS-3: THE FIVE-STORY
PRECAST TEST BUILDING, VOL3-3

by

Sri Sritharan
Iowa State University

Stefano Pampanin
Politecnico di Milano, Italy

James R. Conley
University of California at San Diego

ABSTRACT

This is the third of a series of reports on design, construction, analysis and testing of a five-story precast concrete building under simulated seismic loading, which was conducted in the third phase of the **Pre**cast Seismic Structural Systems (PRESSS) program.

In this report, the design philosophy, verification of design forces, instrumentation details and test procedures of the PRESSS building are presented. The PRESSS building represented a five-story office building at 60% scale and consisted of 2 bays x 2 bays in plan. Two precast frames in one direction and a jointed wall system in the orthogonal direction provided the seismic resistance in the test building. In addition, two gravity frames parallel to the wall system were also modeled. Four precast beam-to-column connection details with different hysteresis behavior, developed in earlier phases of the PRESSS program, were used at different levels of the two seismic frames. The wall system contained unbonded prestressing, with special passive energy dissipating devices located in a vertical construction joint between wall panels. The two most popular precast flooring systems, namely the pretopped double tee and topped hollow core, were also used at different levels of the test building. The PRESSS building is thus a test bed for performance verification of precast seismic systems developed in previous phases of the PRESSS program in a complete statically indeterminate building configuration including interactions with floor diaphragms.

Design of the test building was performed based on a direct-displacement based procedure to sustain a target drift of 2% under a design level earthquake, which has an acceleration response spectrum equivalent to that specified in UBC 94 for soil type S2 in Zone 4. An extensive instrumentation scheme was adopted on the PRESSS building which was tested independently in the two orthogonal directions using three different test procedures. This included a significant amount of pseudodynamic testing, in which the building was subjected several earthquake time histories that exercised the building to a series of successive limit states. The other two test procedures evaluated the elastic stiffness and building behavior at the fundamental mode at different limit states. Seismic testing was first conducted in the wall direction and then in the frame direction to drift levels up to twice the design target drift of 2%.

ACKNOWLEDGEMENTS

TABLE OF CONTENTS

LIST OF FIGURES

LIST OF TABLES

CHAPTER 1

INTRODUCTION

PREcast Seismic Structural Systems (PRESSS) is a three phase research program initiated in 1991 by the US and Japan as part of research of the U.J.N.R. Panel on Wind and Seismic Effects Large-Scale Testing. The US part of the PRESSS research, which is jointly sponsored by the National Science Foundation (NSF), the precast/Prestressed Concrete Institute (PCI) and the Precast/Prestressed Concrete Manufacturers Association of California (PCMAC) has two fundamental objectives:

1. To develop new materials, concepts and technologies for precast concrete construction in different seismic zones, and
2. To develop comprehensive and rational design recommendations needed for a broader acceptance of precast concrete construction in different seismic zones.

The Phase I of PRESSS research [1–4] focused on concept development, connection classification and modeling, analytical platform development, preliminary design recommendations and research coordination. In PRESSS Phase II [5], emphasis was placed on the development of ductile-connection precast structural systems through experimental and analytical studies and development of seismic design procedures for precast buildings in various seismic regions. Integrating the components of experimental and analytical research developed in previous phases, PRESSS Phase III was built around large-scale seismic testing of multi-story precast building systems, one with moment-resisting frames and the other containing structural walls. Design and analysis of each building system were performed with assistance from the PRESSS industry advisory group.

Using the prototype dimensions and details, a test building superassemblage appropriate for laboratory testing was established at 60% scale. By subjecting the superassemblage to a series of simulated seismic tests, suitability of different precast systems in seismic design was examined. Reduction of data obtained during various tests and formulation of design recommendation for all precast structural systems used in the PRESSS test building have been completed. Validation of the design recommendations and a codification process for some of these structural systems are currently underway.

Various aspects of Phase III research are presented in a series of PRESSS technical reports. As the third report of this series, design verifications and test plans of the building superassemblage are presented herein.

1.1 Test Building Superassemblage

For establishing the test building, two five-story precast structures proposed by Nakaki and Englekirk [2] were selected as the prototype buildings with identical structural configuration and different flooring systems. Pretopped double tees in the first building and topped hollowcore floor systems in the second building were used. As shown by plan views in Figures 1.1 and 1.2, both prototype buildings, which have 100'x200' in plan and 12'-6" story height, rely on two moment resisting frames in one direction and structural wall systems in the orthogonal direction to provide seismic resistance. A test building was established from these prototype buildings at 60% scale [6], allowing both precast moment resisting frame and wall systems to be investigated in one superassemblage in conjunction with the two flooring systems.

Figure 1.3 shows the typical plan of the first three floors in the test building, which adopted pretopped double tee planks for the flooring system. In the upper two floors, topped hollowcore panels were incorporated as shown in Figure 1.4. The test building consisted of 2 bays x 2 bays in plan, with seismic resistance provided by two precast frames in one direction and a jointed wall system in the orthogonal direction. One of several precast ductile frame connections investigated in the second phase of the PRESSS research program [5] would have been sufficient for seismic frames in the prototype buildings. However, the test superassemblage accommodated two different frames, namely the prestressed frame and TCY (Tension-compression yield) frame with two types of beam-to-column connections per frame as detailed in Table 1.1 and Figures 1.5 and 1.6. Adopting different beam-to-column precast connections in one test building allowed performance verification of several equivalent prototype buildings in one test superassemblage.

Table 1.1 Different beam-to-column frame connections adopted in the test building.

Frame ID	Floors	Connection Type
Prestressed frame	1, 2 and 3	Hybrid connection
Prestressed frame	4 and 5	Pretensioned connection
TCY frame	1, 2 and 3	TCY gap connection
TCY frame	4 and 5	TCY connection
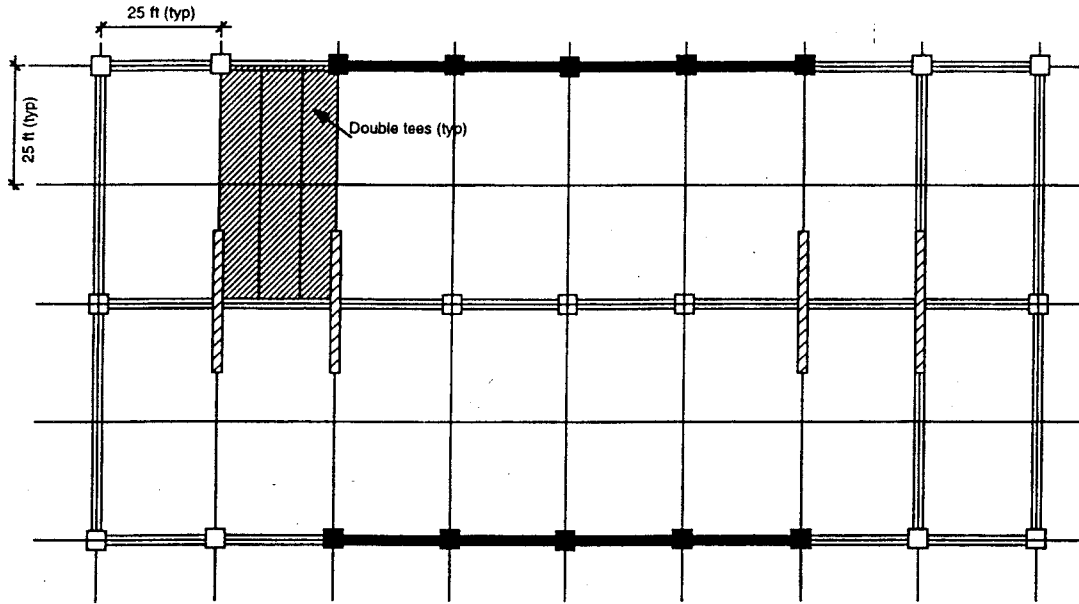
Figure 1.1 Prototype building with pretopped double tee flooring system.
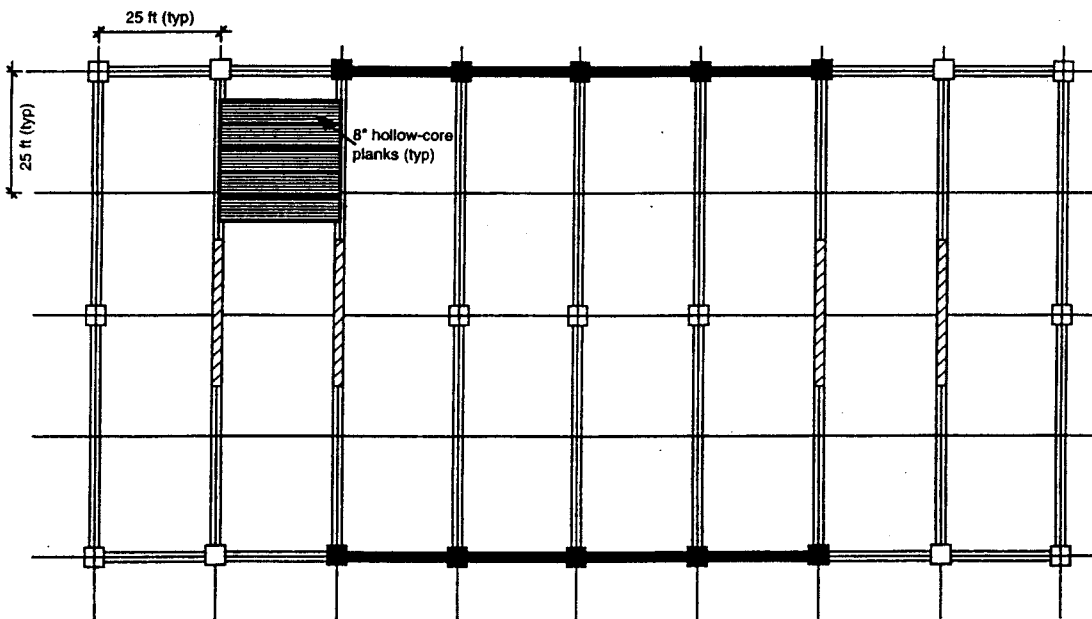
Figure 1.2 Prototype building with topped hollow-core slabs.

Of the four frame connections, multiple bay beams and single story high columns were used in the pretensioned frame connection, while single bay beams and multiple story high columns were used in the other three connections (see Figures 1.5 and 1.6). Brief descriptions of the four beam-column connection details are as follows:

3
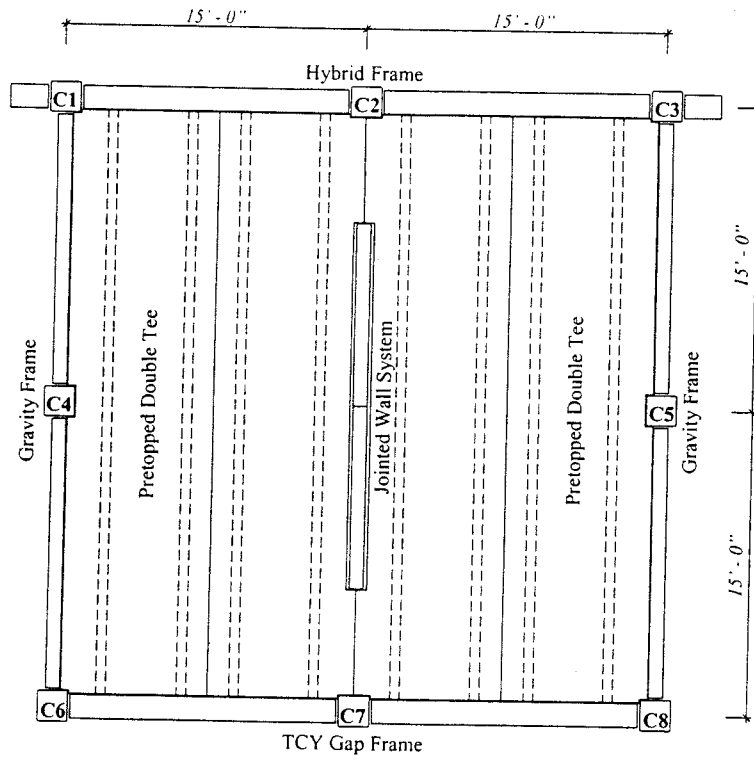
Figure 1.3 Typical plan of the PRESSS building at the first three floor levels.
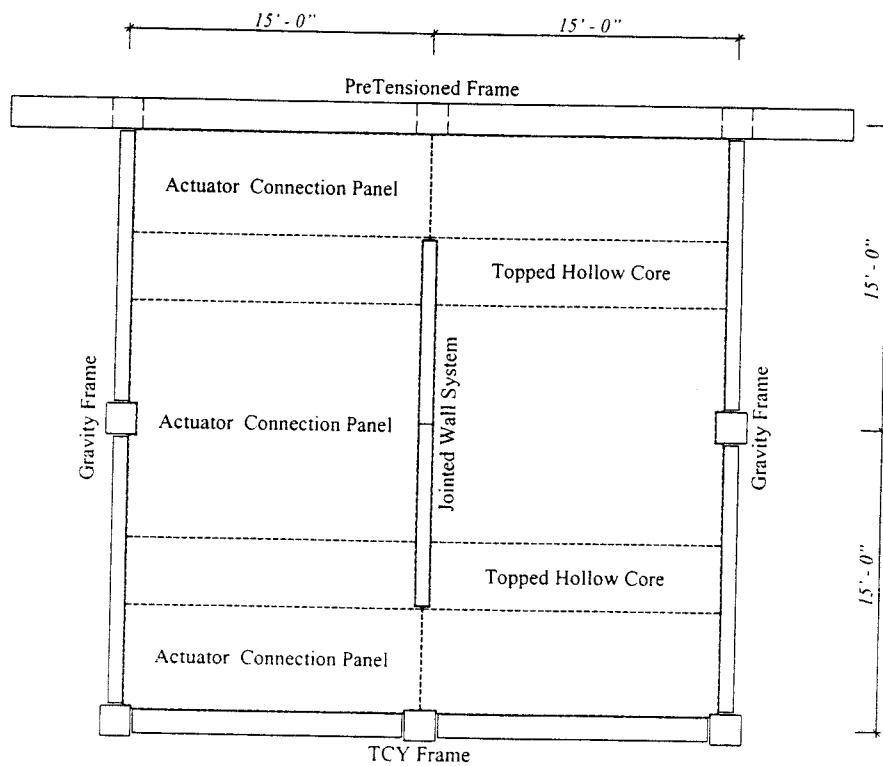
Figure 1.4 Typical plan of the PRESSS building at the upper two floor levels.
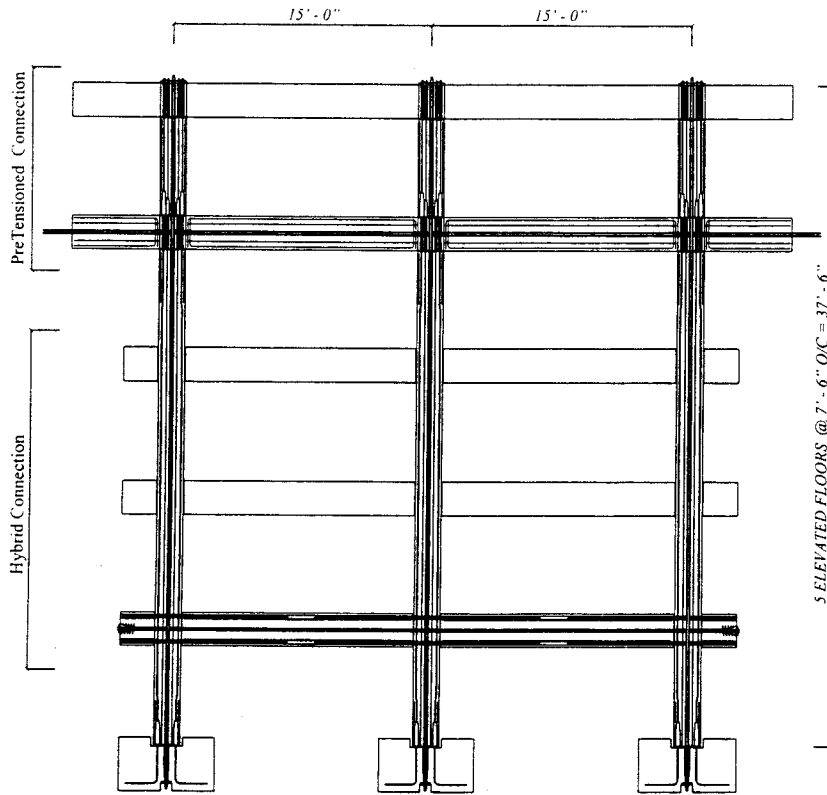
Figure 1.5 Elevation of the prestressed frame.
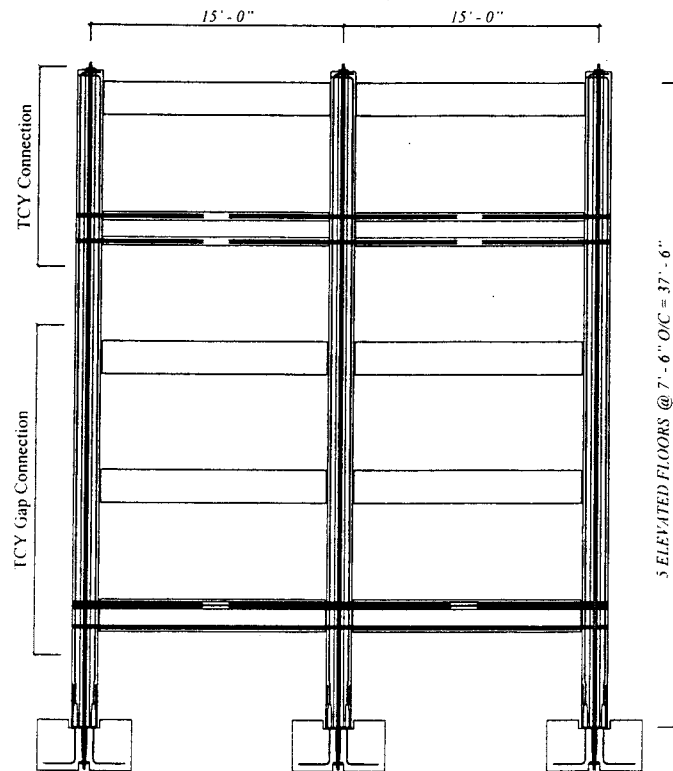
Figure 1.6 Elevation of the TCY frame.

(a) Hybrid Frame Connection

The connection between precast beams and column is established with unbonded post-tensioning through the center of the joint, and field placement of mild steel reinforcement in ducts across the precast joint interfaces close to the top and bottom beam surfaces (Figure 1.7) [7]. The ducts are grouted to ensure adequate bond for the reinforcement prior to post-tensioning. Nonlinear elastic response from the unbonded prestressing steel and hysteretic behavior with energy dissipation from the mild steel reinforcement are expected, resulting in both the ability to dissipate energy and reduced residual displacements for the frame system. In order to reduce accumulation of inelastic strains in the mild steel reinforcement at the critical sections, the reinforcement is debonded over a short length using a thin plastic wrap.
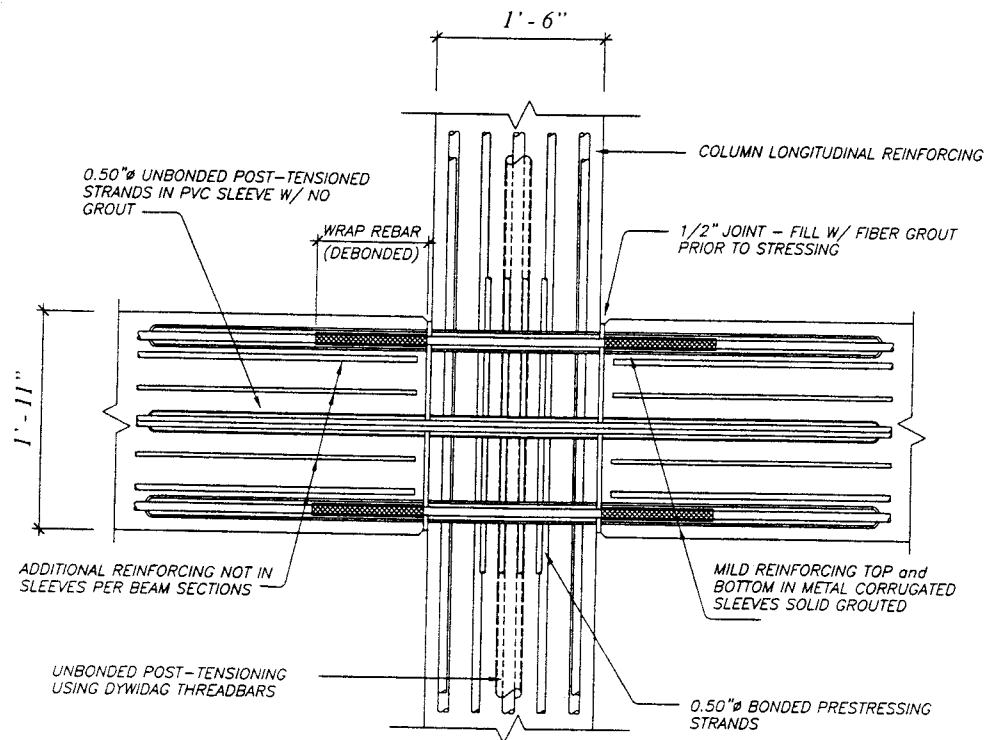
Figure 1.7   Hybrid frame connection of an interior joint in the test building. (Transverse reinforcement in the beams and column are not shown for clarity.)

(b) Pretensioned Frame Connection

In the pretensioned frame, continuous beams are connected to column segments extending from the top of a beam at one floor level to the bottom of a beam at the level

6

above (Figure 1.6) [8]. The moment resistance at the critical beam sections at column faces is provided by pretensioned steel, which is bonded only within the beam-to-column joints and in the beam stubs. The moment connection between the beam and column is established by extending the column mild steel reinforcement below the beam through sleeves located in the joint (Figure 1.8). The extended reinforcement is spliced to the column longitudinal reinforcement at the next level adjacent to the joint. This frame connection is expected to provide almost nonlinear elastic response with a relatively low amount of hysteretic damping. Mild steel reinforcement can be incorporated in the pretensioned connection to enhance the hysteresis behavior, which will provide a system with performance comparable to the hybrid frame connection.
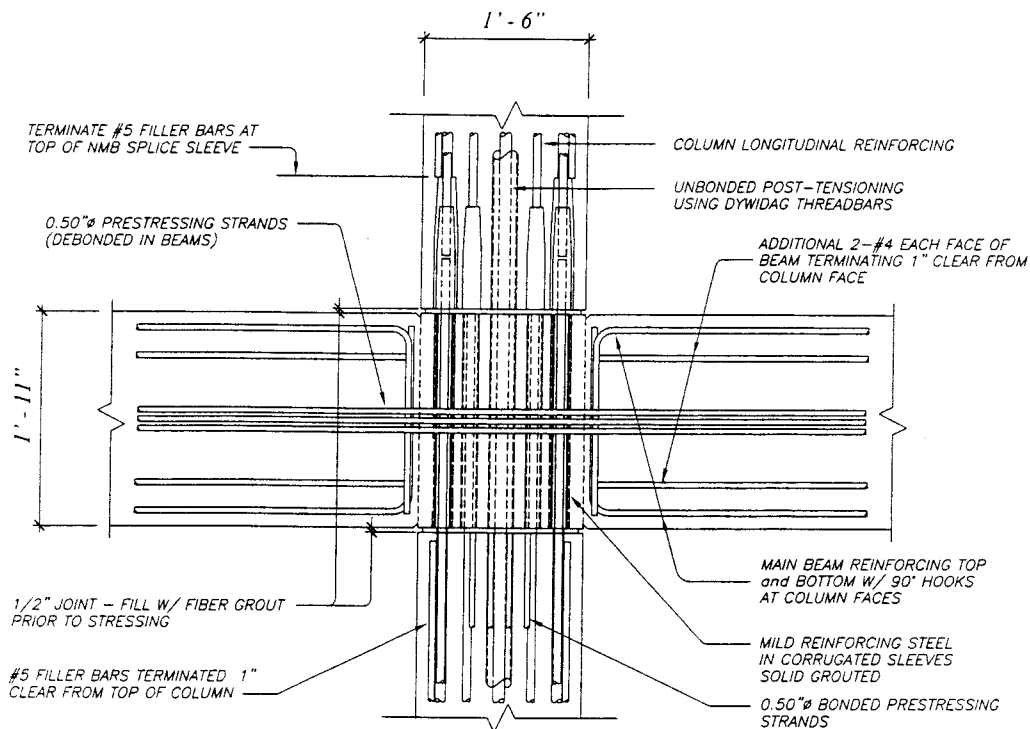
Figure 1.8   Pretensioned frame connection of an interior joint. (Transverse reinforcement in the beam and columns are not shown for clarity.)

(c) TCY Gap Frame Connection

In the TCY gap connection, the beams and columns are separated by a small gap to avoid elongation of the beam due to seismic action [8]. Mild steel reinforcement placed in grouted sleeves at the top of the beam and unbonded post-tensioning at the bottom of the beam provide the moment resistance at beam ends (Figure 1.9). As with

7

the hybrid system, the reinforcement is debonded over a short length to control build up of inelastic strains at the critical sections. The gap between the beam and column is grouted over 6" (i.e., over **0.26h_b**, where **h_b** is the beam depth) at the bottom of the beam with the post-tensioning force acting at the center of grout. In addition to ensuring no significant damage to the beam ends, the gap assures force transfer at the top of the beam only through mild steel reinforcement. As a result, no elongation in the beam is expected even when the reinforcement is subjected to high inelastic strains. Since the mild steel is located only at the top, reduced damping and reduced residual displacements are expected when compared to the TCY connection described below.
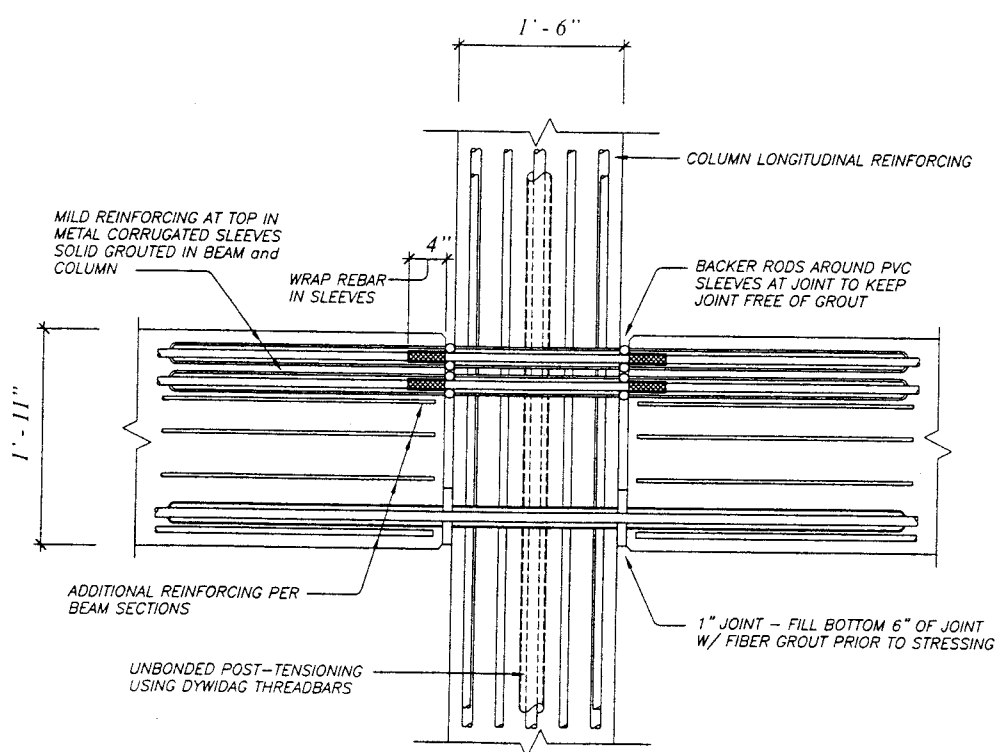
Figure 1.9   TCY-gap frame connection of an interior joint in the test building. (Transverse reinforcement in beams and column are not shown.)

(d) TCY Frame Connection

Behavior of monolithic reinforced concrete connections is emulated in TCY connection with top and bottom mild steel reinforcement in grouted sleeves across the beam-to-column interface (see Figure 1.10). Strain accumulation in the reinforcement is again controlled by debonding the rebars over a short length at the critical sections. The hysteretic actions of this system can provide as high as 35% equivalent viscous damping

8

at large ductilities [5]. However, with such a high damping, higher residual displacements as in cast-in-place concrete would be inevitable when the structure is subjected to large earthquakes. Insufficient shear transfer across the beam-column interface can lead to vertical slip of the beams. Slipping of the beams was monitored in one bay of the TCY frame while steel corbels were installed to improve shear transfer in the second bay (see Vol.3-2 for more details, [9]).
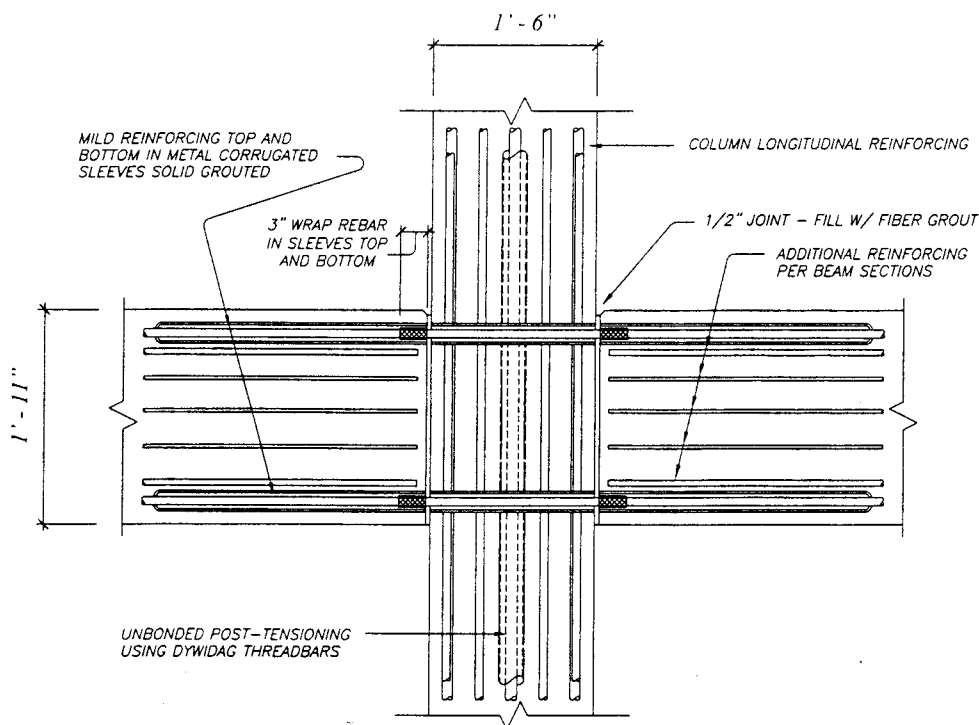
Figure 1.10 TCY frame connection of an interior joint in the test building. (Transverse reinforcement in beams and column are not shown for clarity).

An elevation of the jointed wall system, which provided seismic resistance orthogonal to the frame direction, is depicted in Figure 1.11. As seen in this figure, the wall system consisted of four 2.5 story high (18'-9") precast panels. Continuity between wall panels in the vertical direction was provided through unbonded post-tensioning at the center of the panels. A link between the precast walls in the horizontal direction was established using stainless steel UFP (U-shaped Flexural Plate) connectors located along a vertical joint between the panels. The UFP connectors, as shown in detail in Fig 1.12, also served as passive energy dissipating devices, where hysteric damping was attained by flexural yielding of the U-plates [10].

9
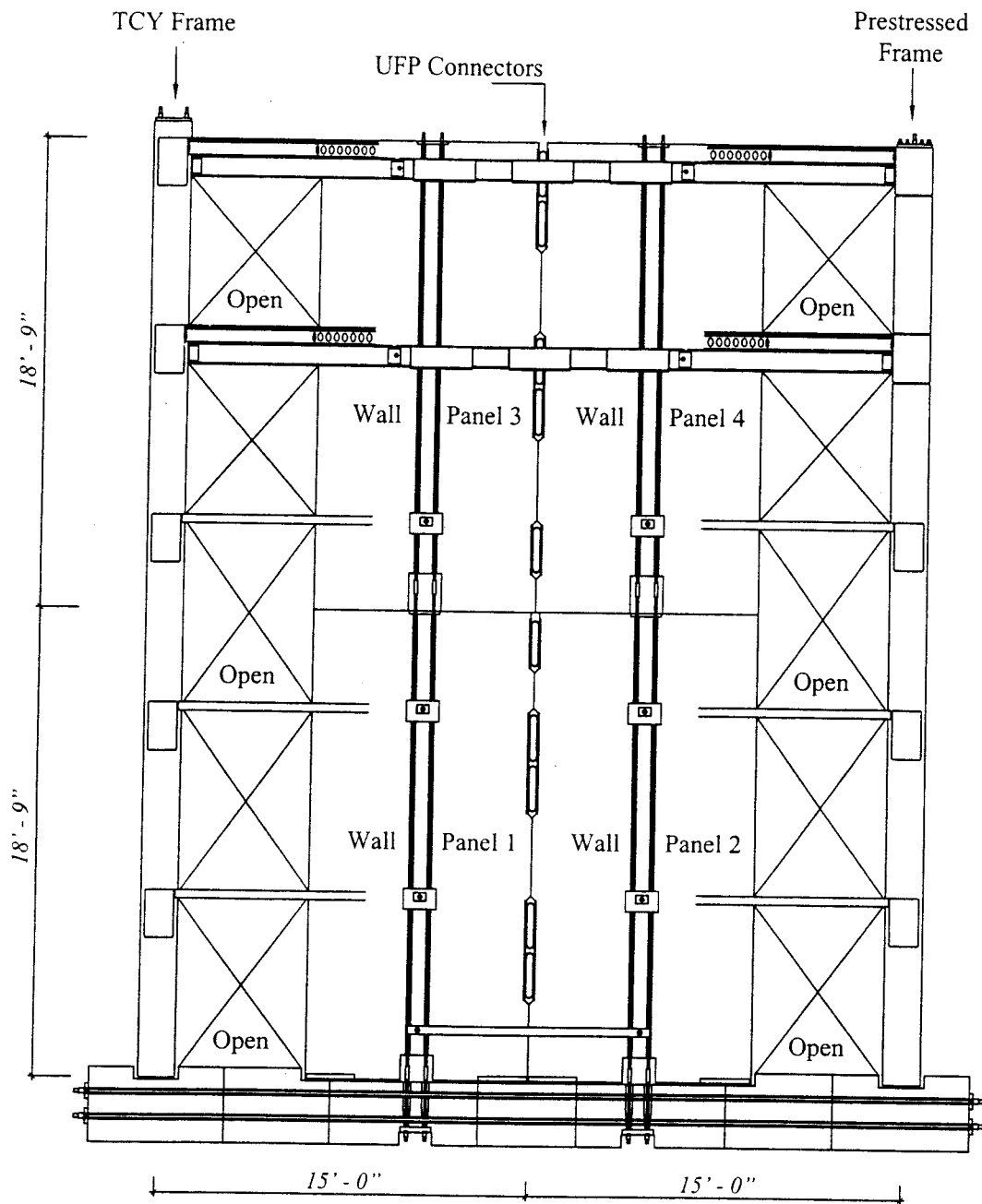
Figure 1.11 Elevation of the jointed precast wall system in the PRESSS building.

The combinations of two building systems, four ductile frame connections, and two flooring systems adopted in the test superassemblage effectively provided experimental verification of seismic behavior of 10 different precast prototype buildings.
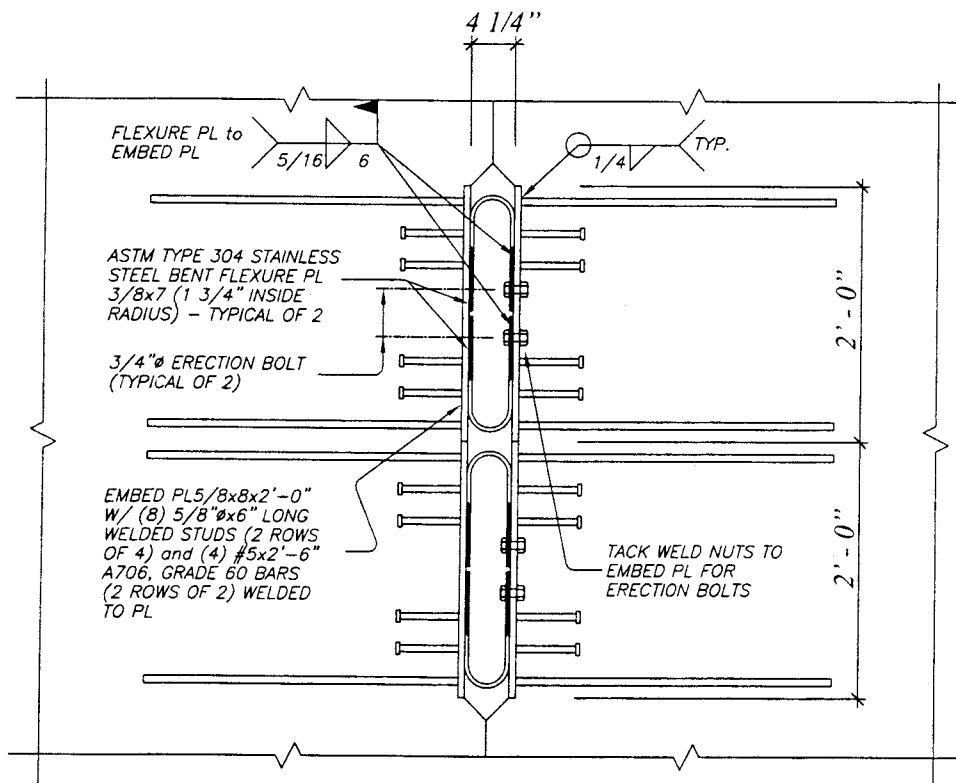
Figure 1.12 Detail of the UFP connector placed in a vertical joint of the wall system.

1.2 Test Objectives

As noted previously, seismic performance of several precast frame and precast wall ductile connections were investigated in the earlier phases of the PRESSS program through component testing. This investigation included examination of the UFP wall connectors and comparable details of the four frame connections used in the test building [6]. The large-scale testing of the precast building superassemblage verified applicability and seismic performance of these ductile connection details in a multi-story building configuration. In addition, the testing of the PRESSS building had the following objectives:

1. To demonstrate the viability of precast concrete design for regions of moderate to high seismicity;

2. To establish dependability of performance of properly designed precast concrete buildings under seismic response;

3. To emphasize the advantages of precast concrete seismic performance when compared to equivalent reinforced concrete or steel structures;

4. To verify and emphasize the advantage of the direct-displacement based design methodology for multi-degree-of-freedom precast structures;

5. To experimentally validate the force transfer capabilities of floor-to-frame, floor-to-wall and floor-to-floor connections;

6. To demonstrate adequate details of the gravity frames, which are not part of the building system resisting lateral seismic forces;

7. To establish predictability of behavior of precast concrete buildings using state-of-the-art analytical tools;

8. To verify the predicted levels of dynamic amplification of column and wall moments and shear forces during seismic response of precast buildings; and

9. To develop design guidelines for precast concrete structures in seismic zones, which can be incorporated into the model building codes.
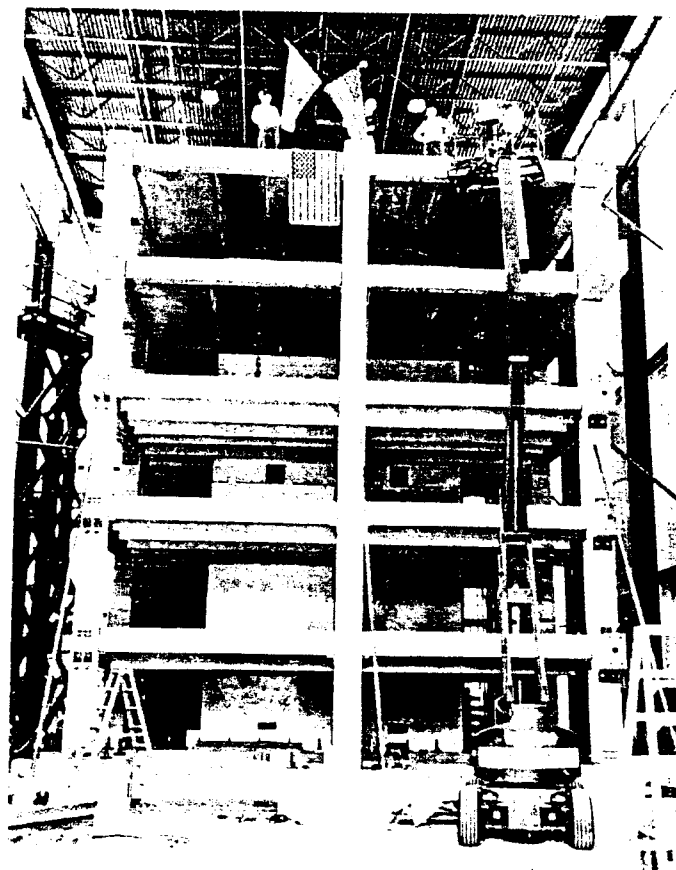
Figure 1.13 The PRESSS test building at the end of construction.

1.3   Construction and Testing

The building superassemblage was constructed and tested in the Charles Lee Powell Structural Systems Laboratory of the University of California at San Diego (Figure 1.13). Following cast-in-place construction of the footings, the test building was assembled using precast components, which were fabricated and delivered to UCSD by various industry representatives involved in the project. Complete details of the construction of the PRESSS building are given in Ref. [9]. The building was tested using different methods, including pseudodynamic testing to several segments of earthquake time histories, the effects of which exercised the building to a series of successive limit states. An extensive instrumentation scheme was adopted to record the seismic behavior of the test for the test building.

1.4   Report Layout

This report describes an independent check on the design forces and test details of the building superassemblage while design details, construction aspects and the test results are documented in companion reports. In Chapter 2 of this report, design verification of the test building using the direct-displacement based method and comparison with design forces obtained from force based design are presented. The test setup and key instrumentation are discussed in Chapter 3, followed by seismic test details including the earthquake time histories chosen for the pseudodynamic test are presented in the subsequent chapter.

CHAPTER 2

DESIGN VERIFICATION

2.1 Introduction

A team comprised of members from the University of Washington at Seattle and Nakaki Engineering in Santa Ana, California, was responsible for the design and detailing of the test building with input from members of the PRESSS III researchers and industry advisor group. The design of the test building is described in detail in references [11,12]. In this chapter, design base shear forces and member design forces are verified independently. Moment demands in various frame members are compared to their capacities established based on the reinforcement details given in reference [11].

2.2 Design Philosophy

Force based design method has been traditionally adopted in seismic design of structures to ensure ductile performance when the structure is subjected to design level earthquakes. This procedure has been incorporated in design codes around the world. Since this methodology is based on elastic acceleration response spectra and force reduction factors, which are somewhat arbitrary and vary between design codes for a given structural type, an alternative procedure based on displacement, known as the direct-displacement based design, has been recently investigated by several researchers. In this procedure, the traditional force based design procedure is completely reversed and the structure is designed for a given drift level using inelastic displacement spectra. Since seismic damage can be better correlated to structural displacements, the displacement based approach was considered to provide a test structure suitable for performance verifications under different levels of seismic loading. It was also recognized that the force based design procedure was not sophisticated enough to take advantage of unique properties of precast systems consisting of ductile connections, whereas this was feasible in the direct-displacement based approach [5].

Consequently, it was decided that structural design of the test building be performed using the direct-displacement based procedure (DDBD) established for multistory buildings at the University of California, San Diego (UCSD) [13,14]. The base

14

shear design forces are also calculated in this chapter using the forced based design, and the values are compared with those determined from the direct-displacement based approach.

The different degrees of protection provided to the precast test building in the direct-displacement based design approach can be summarized as follows:

- *Service Limit State:* When subjected to small relatively frequent earthquakes, the structure should respond with little or no damage, preserving its functionality. No repair should be necessary.

- *Damage Control Limit State:* In moderate earthquakes, yielding of reinforcement and minor repairable damage are permitted in the structure.

- *Design Limit State:* In design level (or large) earthquakes, a maximum inter-story drift of up to 2% is achieved with repairable damage needing injection of grout and replacement of loose concrete.

- *Survival Limit State:* In severe earthquakes including the maximum considered event, structural collapse must not occur, but extensive damage to the structure is permitted. The repair of the structure is still feasible, but is not necessarily economical.

2.3   Design Procedure

As noted previously, the direct-displacement based design procedure established for multi-storey building by researchers at UCSD is adopted for the design of the test building superassemblage. This procedure can be summarized as follows.

- For a given design drift, θ_d, the displacement profile along the height of the building is approximated using Eqs. 2.1 or 2.2. When deriving these equations, the critical location for θ_d is assumed to be at the lower floors for building frames and at the top floor for wall structures (Figure 2.1).

$$\Delta_i = \theta_d h_i \left[1 - \frac{0.5(n-4)h_i}{16h_n} \right] \quad \text{- for frames with } 4 \leq n \leq 20 \qquad (2.1)$$

$$\Delta_i = \frac{2}{3} \frac{\varepsilon_y}{l_w} h_i^2 \left[1.5 - \frac{h_i}{2h_n} \right] + \left[\theta_d - \frac{\varepsilon_y h_n}{l_w} \right] \left[h_i - \frac{l_p}{2} \right] \quad \text{- for walls} \qquad (2.2)$$

15

where h_i is the story height, h_n is the total height of the building, n is the number of stories, l_w is the length of the wall, l_p is the theoretical plastic hinge length, and ε_y is the yield strain of the main longitudinal reinforcement in the wall.

Structure	Displacement	Structure	Displacement
(a) Frame type		(b) Wall type	
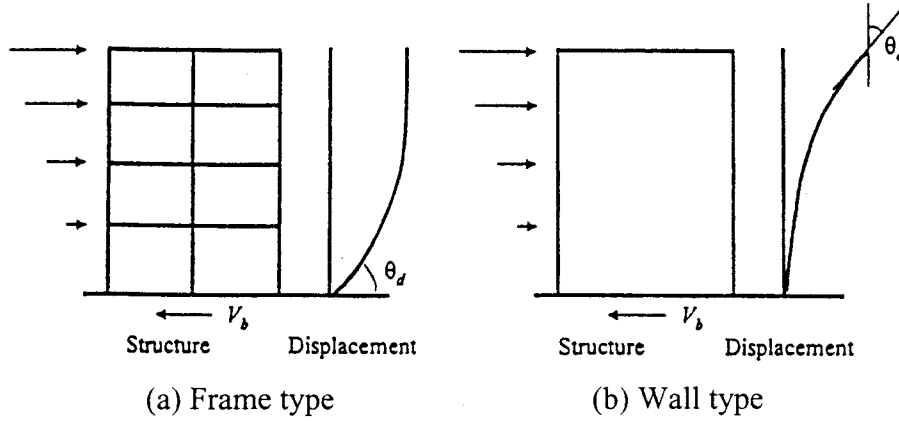
Figure 2.1 Critical lateral drift in building structures [14].

- The multi-degree freedom system is characterized with an equivalent single degree of freedom system (Figure 2.2a). The target displacement and effective mass of the single degree of freedom system are obtained using Eqs. 2.3 and 2.4, respectively.

$$\Delta_d = \left[\frac{\sum_{i=1}^{n}\left(m_i \Delta_i^2\right)}{\sum_{i=1}^{n}\left(m_i \Delta_i\right)} \right] \tag{2.3}$$

$$m_e = \frac{\sum_{i=1}^{n}\left(m_i \Delta_i\right)}{\Delta_d} \tag{2.4}$$

- Using an expected equivalent viscous damping of the structure and value of Δ_d from Eq. 2.3, the effective period, T_e, is obtained from a suite of design displacement spectra as illustrated in Figure 2.2.

- The effective stiffness of the single degree of freedom system and the base shear are obtained from the following equations.

16

(a) SDOF Simulation   (b) Effective stiffness, K_e

(c) Equivalent damping vs. ductility   (d) Design displacement response spectra
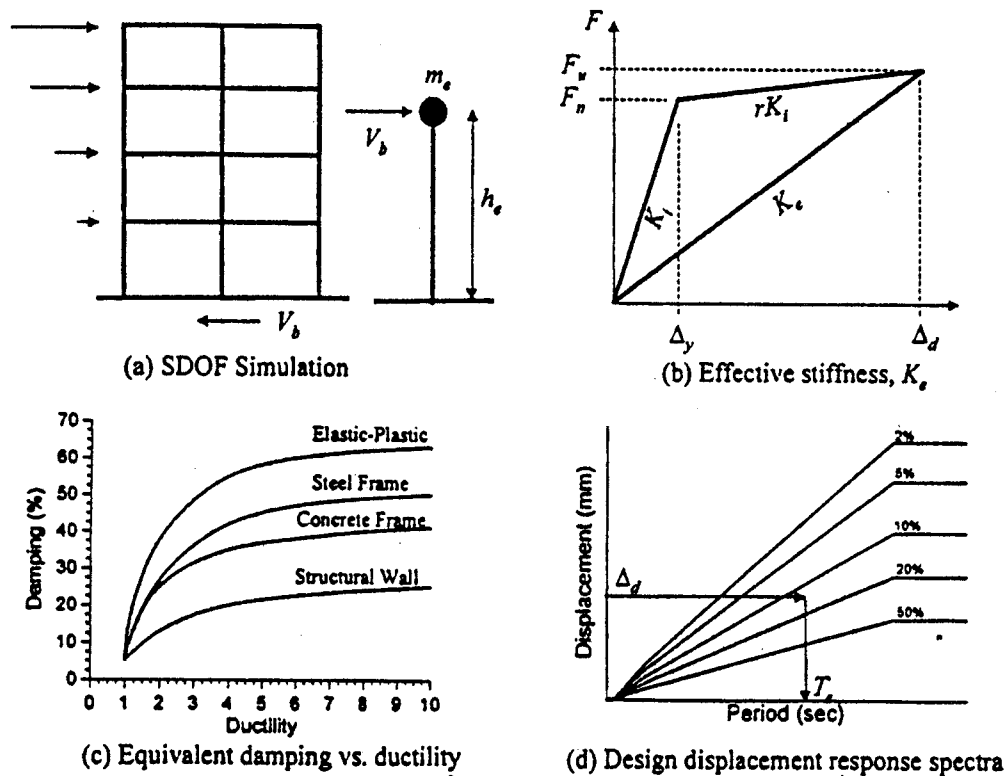
Figure 2.2 Summary of the direct-displacement based approach [14].

$$K_e = 4\pi^2 \frac{m_e}{T_e^2} \qquad (2.5)$$

$$V_b = K_e \Delta_d \qquad (2.6)$$

The above procedure was applied to the prototype buildings rather than directly to the test building. The design base shear of the test building was obtained by scaling down the base shear obtained for the prototype buildings to account for the reduced dimensions of the test structure. Member design forces in the test building were estimated using the dimensions and base shear of the five-story precast test building. The first part of the outlined design procedure for obtaining base shear of the test building is similar to that adopted by the design team. However, the design team opted for obtaining member design forces in a similar fashion by calculating the values for the prototype structure and reducing them to the test building to respect the scale differences [11].

17

2.4 Target Displacement, Damping and Design Spectra

The critical elements required in the direct-displacement based design are dealt with in this section, and the base shear calculations are presented in the subsequent sections. Seismic design of the precast prototype buildings was intended to be in accordance with the 1994 Uniform building Code (UBC) spectrum for soil type S2 [14]. The 1994 UBC, which adopts the forced based design approach, provides elastic acceleration response spectra for three soil types namely S1, S2 and S3 and the corresponding displacement spectra were not provided. The code acceleration spectra were not meant for conversion into displacement spectra and thus a realistic suite of displacement spectra could not be established from this design code.
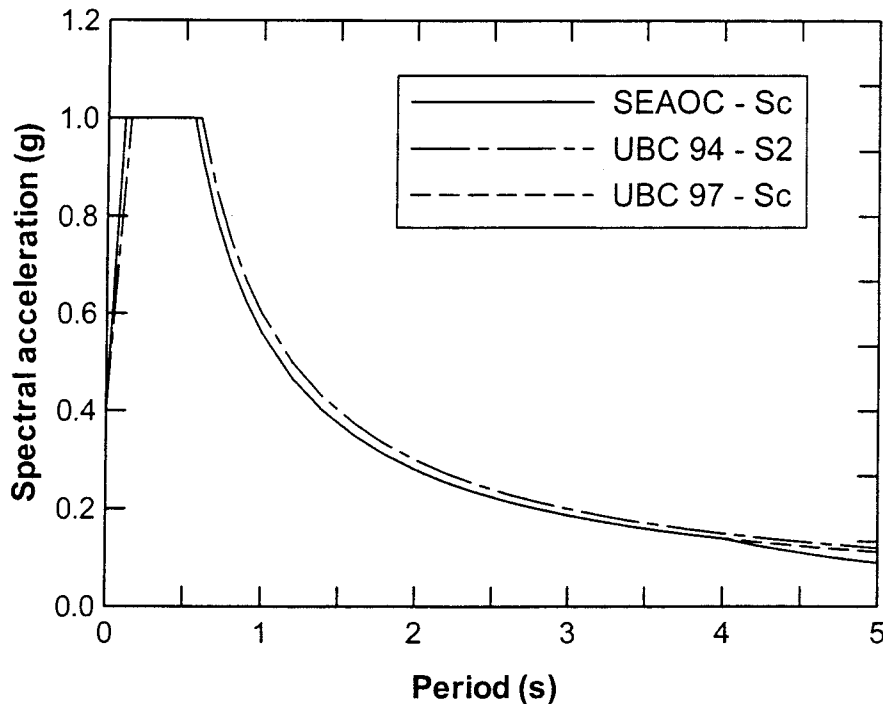
Figure 2.3 Acceleration response spectra corresponding to 5% damping.

An effort to establish displacement response spectra suitable for seismic assessment and design has been made by the performance based design committee of the Structural Engineering Association of California (PBE-SEOAC) [16]. Using the acceleration response spectra recommended in the 1997 NEHRP provisions [17] as the basis, PBE-SEOAC recommends acceleration and displacement spectra for four levels of earthquakes, representing frequent, occasional, rare and vary rare events. This document

18

classifies the foundation type into five soil classes, from S_A to S_E, which is also identical to the NEHRP provisions. For design purposes, Level III spectra are recommended with Level IV events representing the maximum considered earthquakes at 150% of the design level earthquakes. In the design of the PRESSS test building, the PBE-SEOAC Level III (i.e., rare events) spectra corresponding to soil type S_C were used, whose 5% damped accelerations response spectrum is shown in Figure 2.3. Also plotted in this figure are the design spectra from UBC 94 [15] for soil type S2 and UBC 97 [18] for soil type S_C. It is seen that the selected design spectrum is comparable to UBC 94 spectrum and is identical to UBC 97 spectrum up to 4.0 second period. At periods beyond 4.0 seconds, the UBC 97 adopts 1/T decay in the spectral values while PBE-SEAOC considers the spectral accelerations in proportion to $1/T^2$ to maintain realistic displacements spectral ordinates at longer periods.

The Level III PBE-SEAOC 5% damped displacement response spectrum for soil type S_C is shown in Figure 2.4 along with the corresponding spectra at different levels of damping. At the time of designing the PRESSS building, a consistent set of displacement spectra as a function of damping was not available in the draft document of Ref. [16]. Consequently, the displacement spectrum for a damping of ζ% was derived from the 5% damped spectrum using the following equation obtained from Eurocode 8 [19].
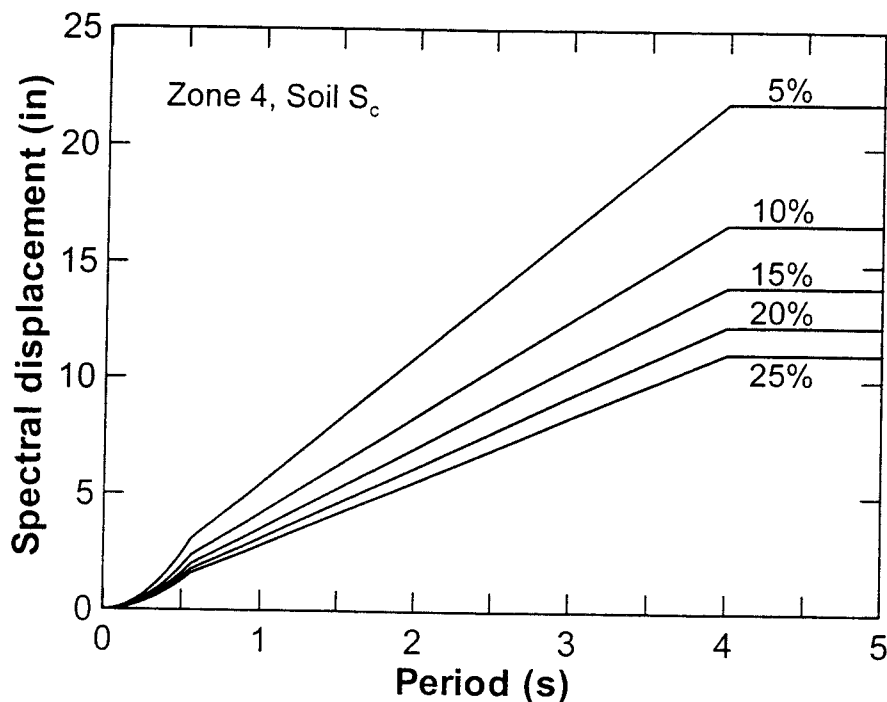
Figure 2.4 Displacement design spectra derived using Eq. 2.7.

19

$$\Delta_{(T,\xi)} = \Delta_{(T,5)}\sqrt{\frac{7}{2+\zeta}} \tag{2.7}$$

The completed PBE-SEAOC document now includes equations for determining spectral points at different levels of damping [16]. In Figure 2.5, the displacement response spectra derived from Eq. 2.7 and that recommended by PBE-SEAOC are compared for the four levels of earthquakes at 20 % viscous damping. For all four levels of earthquakes, it is seen that the displacement spectral ordinates are comparable up to a period of 4.0 seconds, beyond which the Eurocode 8 expression provides lower values than that recommended in Ref. [16].
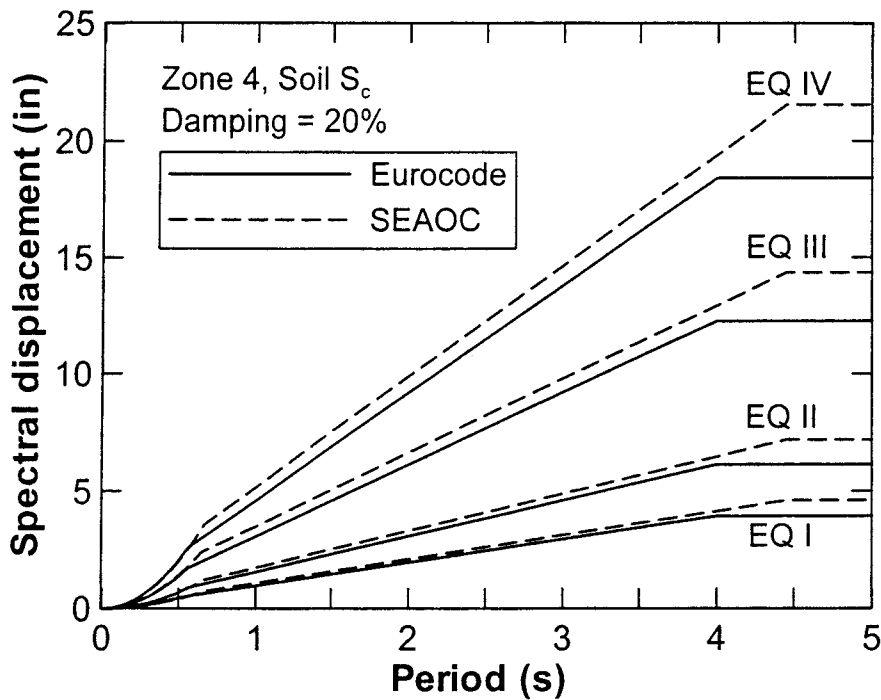
Figure 2.5 Comparison of 20% damped displacement response spectra.

2.5. Wall Design

As previously mentioned, the design base shear was determined at the prototype scale. At a design drift of 2%, an equivalent viscous damping of 12.4% was estimated by the designers [12]. Instead of using Eq. 2.2 for deriving the displacement profile, a linear profile was assumed along the height of the wall. Given the aspect ratio of the wall

system, this assumption was found to be satisfactory. The critical values obtained when establishing the design base shear using the DDBD procedure are listed in Table 2.1. As seen in this table, a design base shear of 2167 kips was obtained in the wall direction which corresponded to 11.1% of the total prototype building weight of 19,500 kips. The design base shear will not be significantly altered if the PBE-SEAOC displacement spectra are used since the ordinates of these spectra at T = 2.878 s are comparable to that derived from Eq. 2.7 up to 4 seconds (see Figure 2.5).

Table 2.1 Estimating the design base shear for the prototype building in the wall direction.

Δ_d (in.)	11.00
M_e (kips/in-s^2)	41.32
T_e (second)	2.878
K_e (kips/in.)	197.0
V_b (kips)	2167

In the test building at 60% scale, only one of the four wall systems in the prototype building was modeled (see Figures 1.1 and 1.3). Hence, the design base shear of the test building in the wall direction was calculated as:

$$2167 \times \frac{1}{4} \times 0.6^2 = 195.0 \text{ kips}$$

This design base shear agrees well with a value of 200.1 kips adopted by the design team.

2.6 Seismic Frame Design

For the response of the two seismic frames combined, an equivalent viscous damping of 20% was estimated at a drift of 2% by the design team by conducting a pushover analysis on a detailed nonlinear analytical model [11]. Due to the differences in hysteresis behavior of the two frames, the prestressed frame was expected to dissipate less seismic energy than the TCY frame when both frames are subjected to equal drifts. The equivalent viscous damping at the design drift was independently examined using relatively a simple analytical model [20]. This study estimated equivalent viscous damping of 14.5% and 20.3% for the prestressed and TCY frames, respectively, which

21

indicated an average damping value of 17.4%. Since the analytical model used by the design team was relatively more sophisticated, the damping ratio of 20% estimated by the design team was used for determining the design base shear.

The direct-displacement based method provided a design base shear of 1508 kips in the frame direction when the displacement spectra shown in Figure 2.4 were used. This base shear is equivalent to 7.6% of the total prototype building weight of 19,500 kips. Estimates of various parameters obtained during this process are listed in Table 2.2. Again note that the effective period of the prototype building was estimated to be less than 4.0 seconds and thus the application of the PBE-SEAOC displacement spectra would yield a comparable design base shear.

Table 2.2   Estimating the design base shear for the prototype building in the frame direction of response.

Δ_d (in.)	10.39
M_e (kips/in-s^2)	40.86
T_e (second)	3.363
K_e (kips/in.)	142.6
V_b (kips)	1482

The four bay seismic frames in the prototype buildings were replaced with two bay seismic frames in the test building at 60% scale (see Figures 1.1 and 1.5). Therefore, the design base shear of each seismic frame in the test building was calculated as:

$$1482 \times \frac{1}{2} \times \frac{1}{2} \times 0.6^2 = 133.4 \text{ kips}$$

This value satisfactorily compares with 132.0 kips estimated by the design team. The sum of the column design base moments obtained from the above base shear would represent the demand on 2.5 columns in the test building due to 50% reduction in the number of bays. Distributing the corresponding total base moment to all three columns forming the two bay frame in the test building, the beam end design moments can be obtained.

In the DDBD procedure for multi-story buildings, the beam end design moments are found by analyzing the frame for a set of lateral loads equivalent to the design base

shear with hinges modeling the column-to-footing connections [13,14]. The moment resistance of the columns at the base was accounted for by applying a resisting moment at the end of each column. Following this procedure, the beam design moments were derived from an analytical model established using computer program RUAMOKO [21]. Details of the model and complete results are presented by Pampanin et al. [20]. A summary of the design moments are listed in Tables 2.3 – 2.7, along with the design strength established from the reinforcement details of the beam-to-column connections.

In order to eliminate any error introduced to the beam end moment comparison by the column base resistance, it was assumed in the pushover model that the column end moment resistance at the design drift was equal to the seismic moment demand (see Table 2.3). The moment demand at the column base was found from the column shear as a function of the column axial force and estimated length from the column end to the inflection point in the first story [14,20]. The reported beam design strengths, which corresponded to the moment resistance at member ends when the frame was subjected to the design drift of 2%, were established by performing pushover analyses on the seismic frames.

Table 2.3 Comparison of moment demand and capacity at the column bases and the corresponding axial forces in each seismic frame.

Identification	Axial Force (kips)	Design Moment (kip-in)	Flexural Strength (kip-in)
Leading column	324.9	2754.1	2754.1
Trailing column	114.8	1538.1	1538.1
Interior column	220.4	2193.0	2193.0

In Tables 2.4 - 2.7, it is seen that the moment demand at the beam ends are less than the design strength in all cases. For the prestressed frame, the design strength was on average 18% higher than the design moments. However, for the TCY frame, a much larger average overstrength of 41% was obtained. There are two reasons for obtaining larger reserve capacities for the beams in the TCY frame. Due to the reinforcement configuration, the TCY gap system inherently has a greater negative moment capacity than the positive moment capacity. As a result, higher overstrength values should be expected when TCY gap beams are subjected to negative moments (see Tables 2.6 and 2.7), which increase the average overstrength factor. If the demand to capacity ratio is

considered only for the positive moments, the average overstrength of the TCY frame reduces to 27%. The second reason, which also explains the estimated average overstrength of 18% for beams in the prestressed frame, is that the beam moment demands estimated by the design team [11] from an analytical model representing the prototype structure were higher than that reported in reference [20], especially in the first two floors. The discrepancies in design moments may be attributed to the differences in the modeling procedure and the choice of analysis method. To a lesser extent, the difference in the first story height between the prototype and model buildings also contributed to the discrepancy in the beam design moments.

The design team used an estimated distribution of beam stiffness along the height of the building with an elastic analysis to determine the design moments [11]. Furthermore, in the test building, the height to the top of the first floor from the column base was 90 inches whereas the corresponding distance in the prototype building was assumed to be to the center of joints located at the first floor level. These differences would have caused the discrepancies in the estimated beam moments. The moment demands estimated by the design team were found to be closer to the beam strengths reported in Tables 2.4. – 2.7, indicating much lower overstrength for the beams in the test building.

From a testing perspective, the higher beam reserve capacities would require higher actuator forces. Given the estimated average overstrength factors for the two frames, it was felt that the total lateral load required at the design level testing and beyond would be well within the actuator force capacities. Therefore, it was decided not to make any changes to the beam reinforcement details in the test building.

Table 2.4   Comparison of moment demand and design strength of beams at the exterior column faces in the prestressed frame.

Floor Level	Positive Moment (kip-in)		Negative Moment (kip-in)	
	Demand	Strength	Demand	Strength
1	2033.9	2727.6	2051.9	2727.6
2	1976.3	2178.9	1971.5	2178.9
3	1724.6	2093.0	1722.2	2093.0
4	1386.4	1573.5	1380.8	1573.5
5	1098.2	1191.2	1090.3	1191.2

Table 2.5　Comparison of moment demand and design strength of beams at the interior column faces in the prestressed frame.

Floor Level	Positive Moment (kip-in)		Negative Moment (kip-in)	
	Demand	Strength	Demand	Strength
1	2018.2	2727.6	2010.0	2727.6
2	1952.9	2178.9	1956.0	2178.9
3	1702.7	2093.0	1705.1	2093.0
4	1371.1	1573.5	1375.8	1573.5
5	1061.1	1191.2	1069.0	1191.2

Table 2.6　Comparison of moment demand and design strength of beams at the exterior column faces in the TCY frame.

Floor Level	Positive Moment (kip-in)		Negative Moment (kip-in)	
	Demand	Strength	Demand	Strength
1	2033.9	2861.2	2051.9	3756.8
2	1976.3	2470.9	1971.5	3331.1
3	1724.6	2024.8	1722.2	2877.1
4	1386.4	1872.7	1380.8	1872.7
5	1098.2	1224.8	1090.3	1224.8

Table 2.7　Comparison of moment demand and design strength of beams at the interior column faces in the TCY frame.

Floor Level	Positive Moment (kip-in)		Negative Moment (kip-in)	
	Demand	Strength	Demand	Strength
1	2018.2	2861.2	2010.0	3756.8
2	1952.9	2470.9	1956.0	3331.1
3	1702.7	2024.8	1705.1	2877.1
4	1371.1	1872.6	1375.8	1872.6
5	1061.1	1224.8	1069.0	1224.8

2.7 Comparison with FBD

Since the design of the precast building was based on the direct-displacement based design, it is of interest to compare the calculated design base shear with that obtained from the force based design method. Table 2.8 provides a comparison for the base shear obtained from the two design methods in the wall and frame directions, with a graphical representation of results in Figure 2.6. As can be seen in the table, the force based design was applied in accordance with UBC 94 [15], UBC 97 [18] and NEHRP 97 [17], and in all cases the forced based design provides a higher design base shear than that estimated from the direct-displacement based design method. The discrepancy in the design base shear obtained from the two methods is greater for the wall system, with FBD producing values 80 – 100% higher than that required by DDBD. The corresponding range for the frame system is 13 – 95%. Reduction of base shear obtained from the direct-displacement based design indicates cost saving expected from the alternative design procedure.

Table 2.8   Comparison of the design base shear obtained from DDBD and FBD at the prototype scale.

Design Method	Code	Wall Direction Base Shear (kips)	Frame Direction Base Shear (kips)
DDBD	PBE-SEAOC with Eq. 2.7	2167	1482
FBD	UBC 94	3900 $(C_t = 0.02, R_W = 6)$	1671 $(C_t = 0.02, R_W = 12)$
	UBC 97	4333[*] $(C_t = 0.02, R = 4.5)$	2887 $(C_t = 0.02, R = 8.5)$
	NEHRP 97	3900 $(C_t = 0.02, R = 5)$	2438 $(C_t = 0.02, R = 8.0)$

[*]Governed by the maximum recommended value
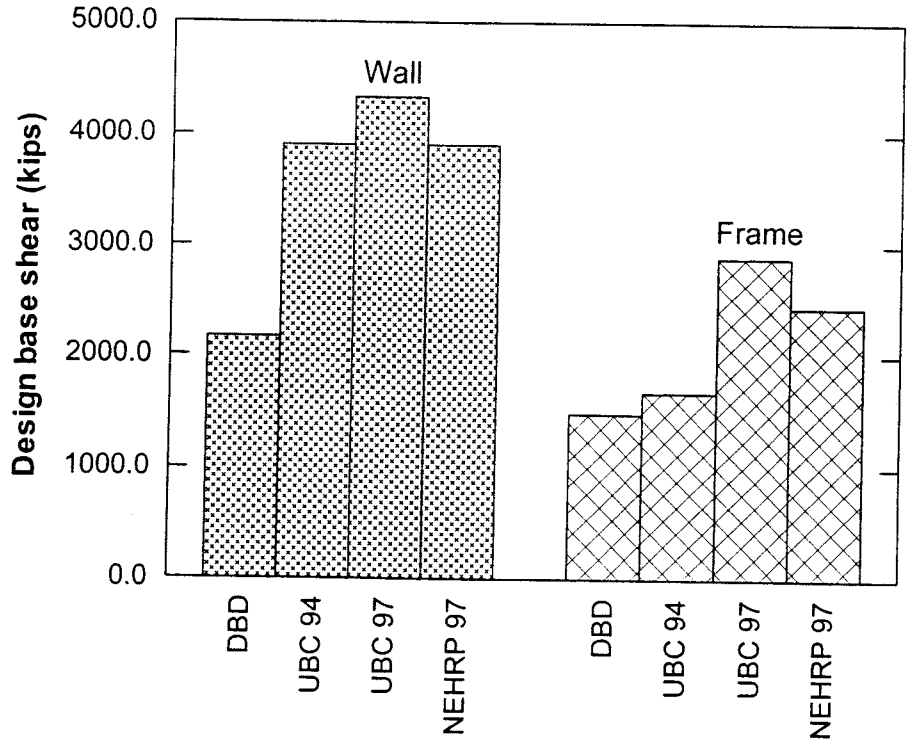
Figure 2.6 Comparison of design base shear obtained from DDBD and FBD.

CHAPTER 3

TEST SETUP AND INSTRUMENTATION

The 60% scale PRESSS building superassemblage described in the previous chapters was constructed and tested at the Charles Lee Powell Structural Systems Laboratory of the University of California, San Diego, (UCSD). The precast components of the superassemblage were fabricated and delivered to UCSD by five different precast manufacturers in California. Following construction of cast-in-place footings, the test building was erected as typically done in the field by a professional erector. Construction details of the building are documented in a companion report [9]. In this chapter, the test setup and instrumentation details of the PRESSS building are presented.

When a multi-story building is subjected to an earthquake ground motion, mass proportional inertia forces are generated primarily at floor levels. Therefore, lateral force simulation was performed for the test building by transmitting appropriate forces at floor levels using 10 servo-controlled hydraulic actuators. A pair of actuators positioned at equal distances from the centerline of the building at each floor level simplified controlling of tests, and aided with eliminating response of the building being influenced by torsional modes. Significant influence of torsion was possible in the frame direction due to the difference in stiffness of the two seismic frames. Accidental eccentricity could have also introduced torsional modes in the two directions of testing.

Seismic testing of the building was first performed in the wall (east-west) direction, followed by testing of the seismic frames in the orthogonal direction (north-south) direction.

3.1   Testing in the Wall Direction

Described below are the applied gravity loads and simulated lateral seismic forces during testing of the wall panel system shown in Fig. 3.1. The wall panel was designed with unbonded post-tensioning, which provided the continuity between precast wall panels in the vertical direction, the required stiffness for the wall system when subjected to lateral loads, and served as the tension reinforcement necessary for developing moment resistance at the base of the wall panels.

3.1.1 Gravity Loads

An objective in scale testing of structures is to replicate the expected prototype stresses and strains in the critical members of the test model. Since the density of the material remains the same in both the model and prototype structures, the gravity effects will not be satisfactorily accounted for unless additional gravity loads are applied to the test models. Non-structural elements are typically not modeled in structural testing, whose axial load effects should also be added to the critical members in the test models. Although testing of the PRESSS building was done at 60% scale without modeling non-structural elements, no additional gravity loads were applied to the wall panels. This decision was motivated by the presence of near full-scale floor panels in the upper two stories of the test building. The weight of the floor panels supported by the wall system satisfactorily represented the additional required gravity loads for a prototype structure designed only with double-tee floor panels as shown in Fig. 1.1. However, for a prototype structure using hollow-core panels as in Fig. 1.2, additional gravity effects should be simulated. Since the change in base moment resistance due to this additional gravity effects was expected to be small and simulation of this load would have required anchoring of more prestressing bars through wall panels, testing of the wall system was performed without applying any additional gravity loads.

Figure 3.1 Construction of the jointed wall panel system.

For the gravity load differences expected in scale testing as described above, additional axial loads were required in the gravity and seismic columns, which were simulated using two unbonded Dywidag prestressing bars in each column. The required additional column axial loads are listed in Table 3.1. In order to minimize any potential damage and the contribution of the lateral force resistance of the seismic columns during the wall direction of testing, only 30% of the required axial loads in Table 3.1 were applied to the seismic columns. The gravity columns were subjected to the total prestressing of 114.8 kips. Furthermore, the splice sleeves provided at the base of the seismic columns were not grouted until after the testing in the wall direction was completed [9]. These splice sleeves were designed to ensure continuity between the column main reinforcing bars and the starter bars placed in the foundations.

Table 3.1 The required column axial loads to simulate gravity effects.

Column ID	Description	Axial Load (kips)
C1,C3,C6,C8	Exterior seismic columns	167.2
C2,C7	Interior seismic columns	114.8
C4,C5	Gravity columns	114.8

3.1.2 Seismic Load Simulation

The UCSD structural systems laboratory, in which the PRESSS building was erected, did not have a lateral force reaction system necessary to simulate seismic forces in the wall direction of testing. Following considerations of various alternative choices, a precast concrete cantilevered loading tower with unbonded prestressing was built. The tower consisted of nine H-shaped precast cells with a two feet cap at the top, totaling 47 ft in height (Fig. 3.2). The cells were designed with wire-mesh reinforcement sufficient to control shrinkage cracks while the cap was heavily reinforced. Some additional reinforcement was also placed in the top cell. The moment
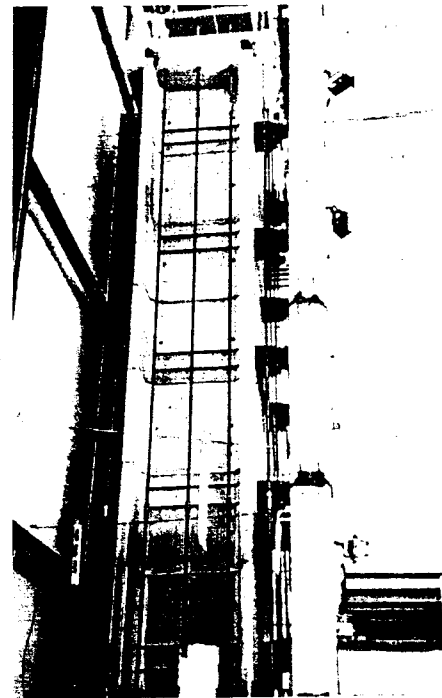
Figure 3.2 The precast loading tower.

30

resistance at the base of the tower was relied on the external post-tensioning of 4000 kips in total, which was applied using 20, 1¼ in. diameter Dywidag bars. This prestressing corresponded to a decompression base moment of 99,250 kips-in. This moment was found to be 36% higher than the expected base moment when the design base shear of 195 kips was applied in the wall direction using an inverse triangular distribution along the height of the PRESSS building.

An elevation and a plan view of the test setup in the wall direction of testing are schematically shown in Figures 3.3 while photographs of the test setup are shown in Figures 3.4. As noted previously, two servo-controlled hydraulic actuators per floor were used for the seismic force simulation. Each of the actuators was connected to the loading tower at one end and to the flooring system at the other end through two pin-connected loading arms (Figures 3.4b-c). The purpose of splitting the actuator force at the floor level was to adequately examine competence of the wall-to-wall, floor-to-wall, floor-to-floor and floor-to-frame connections. At each floor level, the actuators were positioned eight feet apart horizontally and 14 inches vertically from the top of the floors to the centerline of the actuators. The loading apparatus included an extension arm such that the center of stroke of the actuator aligned with the center of loading points on the floors. Details of the different lateral load tests and seismic input motions are given in Chapter 4.

3.2   Testing in the Frame Direction

Gravity loads in the columns and lateral forces parallel to the seismic frame direction were simulated as follows.

3.2.1   Gravity Load Simulation

The axial loads in the wall system and gravity columns were not altered following completion of seismic testing in the wall direction. The axial loads in the seismic columns were increased to match the target values listed in Table 3.1.

3.2.2   Seismic Load Simulation

Lateral forces in the seismic frame (i.e., north-south) direction were simulated with respect to the laboratory strong wall (see Figures 3.4d and 3.5). As with the wall direction, two actuators per floor were used and the actuator forces were transmitted to the floors through two loading arms as detailed in Figure 3.4b and 3.4c.
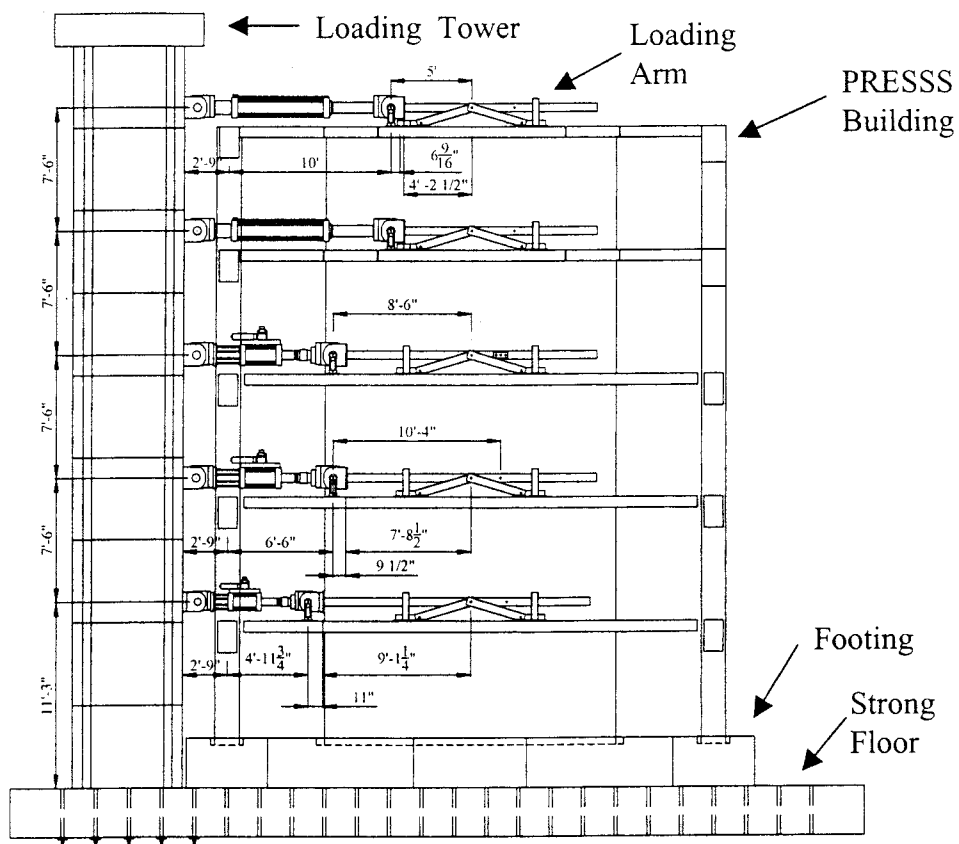
(a) Elevation
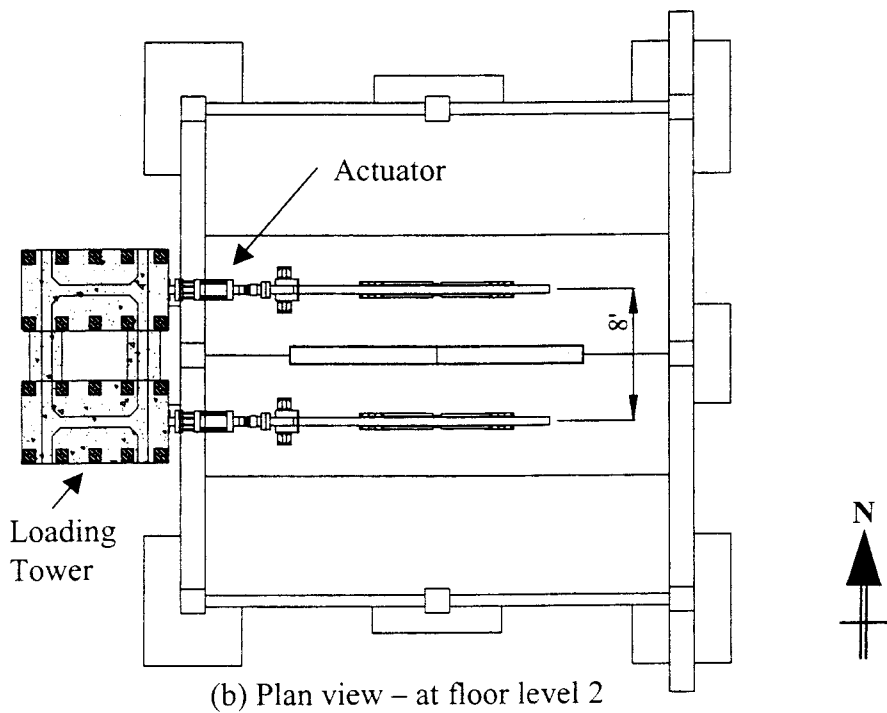
(b) Plan view – at floor level 2

Figure 3.3 Schematic view of the wall direction of testing.
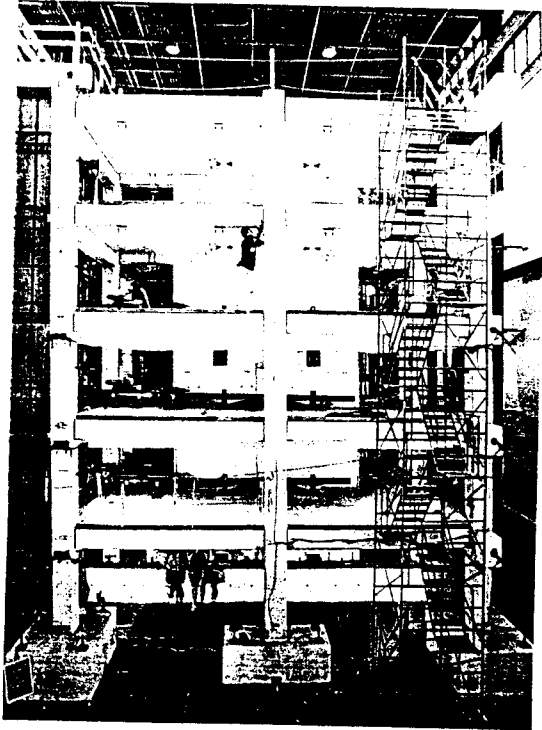
(a) Testing in the wall direction
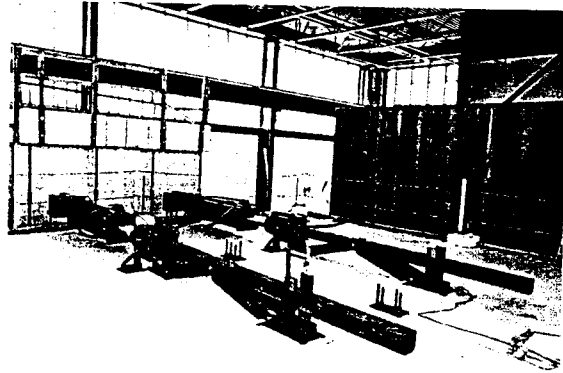
(b) Actuators mounted on the top floor in the wall direction testing
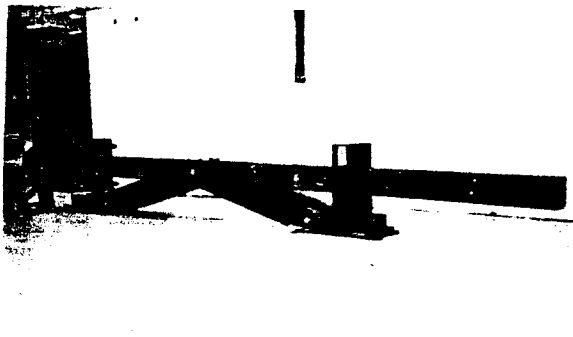
(c) Actuator loading arm
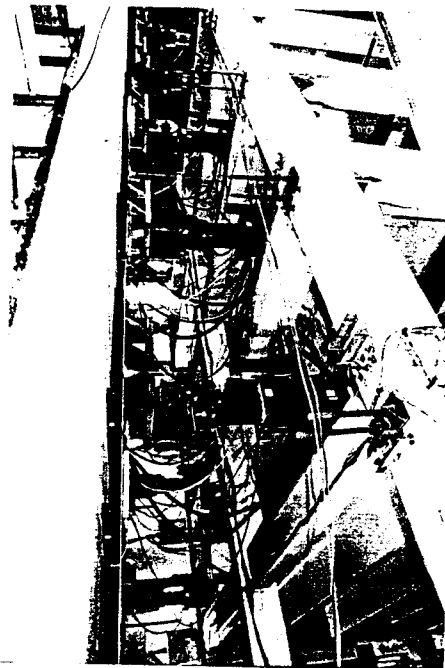
(d) Frame direction of testing against the strong wall

Fig. 3.4 Testing of the PRESSS building.

The actuators were again positioned at 14 inches above the top of the floors, but at 22 ft apart in the horizontal direction. Details of the different lateral load tests and seismic input motions are given in Chapter 4.

33
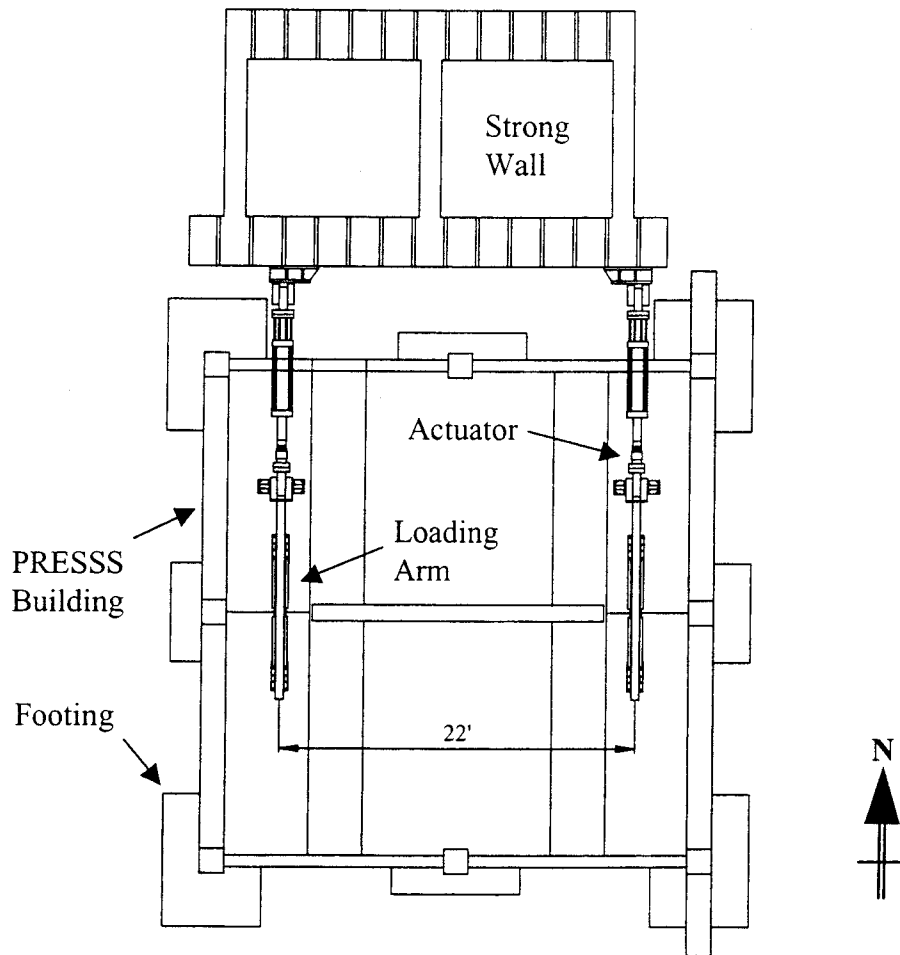
Figure 3.5 A plan view showing testing in the frame direction.

3.3 Details of Instrumentation

An instrumentation scheme consisting of strain gauges, displacement transducers, rotation devices, curvature cells and joint panel devices was designed to capture the seismic response characteristics of the PRESSS building. The majority of the strain gauges were mounted on the mild steel and prestressing reinforcement at the critical locations, and on the UFP connectors. The gauge locations are summarized for each direction of testing in the subsequent sections. Lateral displacement of the structure at various locations with respect to reference points were monitored using displacement transducers. In addition, relative displacements between various precast elements and change in overall length of the seismic beams were also recorded.

34

Strain gauges, displacement transducers and rotation devices recorded the required data directly while interpretation of instrument readings was necessary for curvature cells and joint panel devices. Details of the latter two devices and associated data interpretation procedures are discussed below.

Curvature cells, each consisting of two linear potentiometers, are typically used to measure an average curvature occurring over a segment of a structural member due to flexural action as illustrated for a column and beam end region in Figure 3.6. With reference to this figure, the curvature can be determined from the displacement measured in one potentiometer with respect to the other as follows:

$$\phi = \frac{\text{rotation}}{\text{gauge length}} = \frac{(\Delta_2 - \Delta_1)/l_w}{l_g} \tag{3.1}$$

where $(\Delta_2 - \Delta_1)$ represents the relative extension within the curvature cell, l_w is the distance between the two potentiometers and l_g is the gauge length. A modified gauge length as given by Eq. 3.2 is recommended to account for strain penetration when a curvature cell is placed adjacent to a beam-column joint (Figure 3.7) or foundation (Figure 3.6) with high inelastic strains developing in the member longitudinal reinforcement at the interface [22].

(a) at column base   (b) at beam end
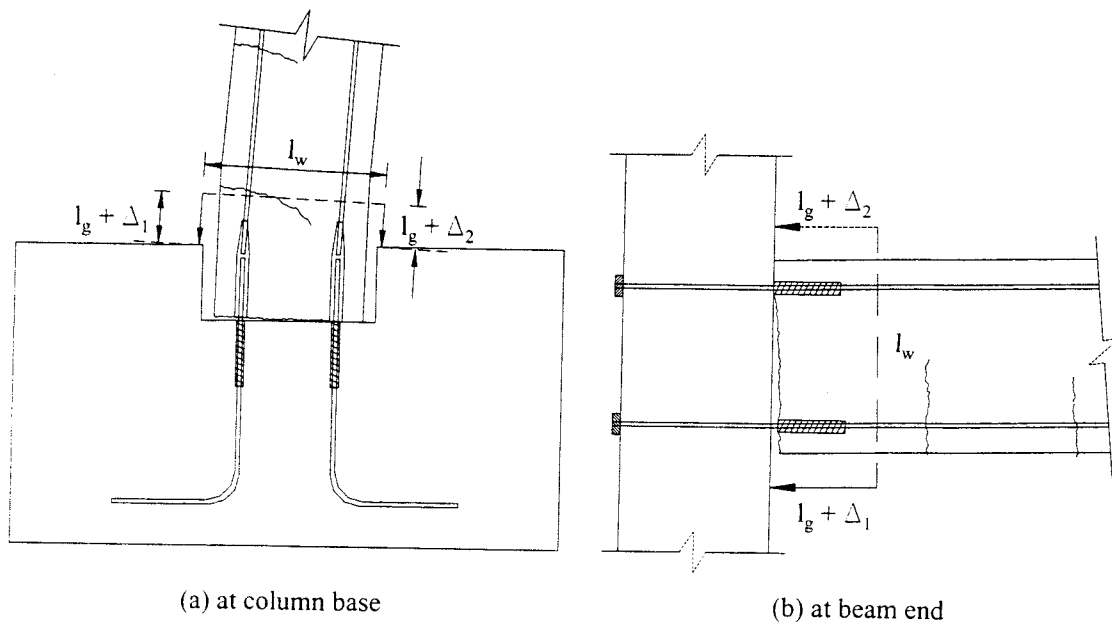
Figure 3.6 Curvature cells mounted at member ends.

$$l_g' = l_{sp} + l_g\left(1 - 1.67\frac{l_g}{l_c}\right)$$
(3.2)

where l_{sp} is the equivalent strain penetration length taken as $0.15f_yd_{bl}$, f_y and d_{bl} are, respectively, the yield strength and bar diameter of the longitudinal reinforcement, and l_c is the distance from the critical section to the point of contraflexure.

Most of the curvature cells in the PRESSS building were mounted across precast joint interfaces where cracking was concentrated in order to protect the precast members from being subjected to significant curvature and subsequent damage (see Figures 3.6 and 3.7). As a result, calculation of an average curvature using Eq. 3.1 for the cells mounted in the test building would be inappropriate. Instead, calculating the rotation of members over the gauge length would be more meaningful. This rotation at a precast member end is primarily due to opening of the crack at the joint interface with a small contribution due to elastic deformation of the structural member over the gauge length.
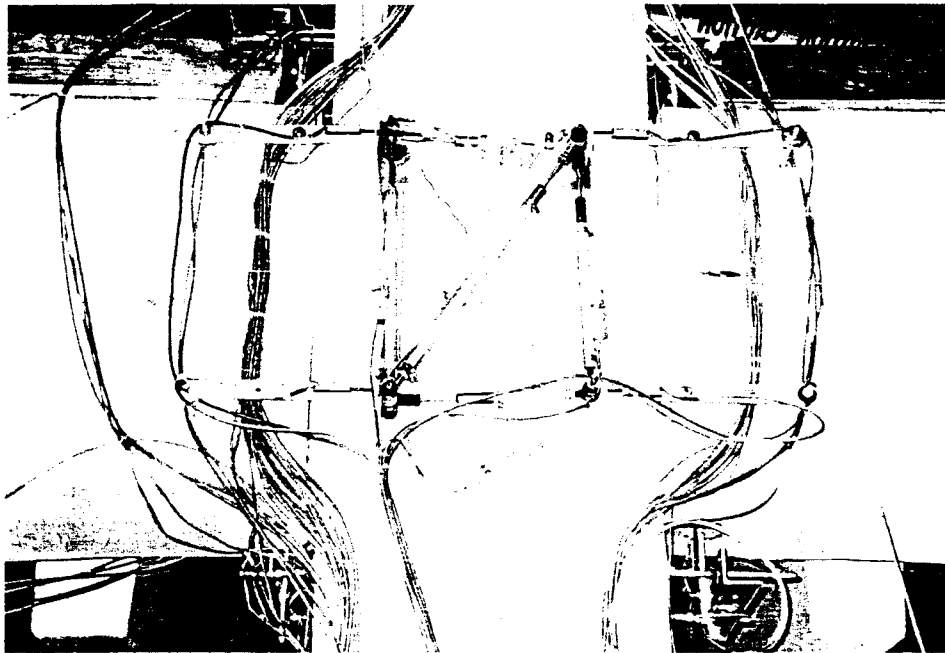
Figure 3.7 Typical instrumentation in a joint panel region.

The panel device, consisted of five linear potentiometers, was used to measure the deformation of a beam-column joint region (see Figure 3.7). When a joint is subjected to

36

a combination of in-plane axial forces and flexural and shear actions, the resulting joint deformation is composed of five independent modes, namely extension in x and y directions, and flexural deformation in x and y directions, and pure shear, as shown in Figure 3.8. These independent joint deformations can be established from the potentiometers measuring relative displacements between joint nodes. From the potentiometer readings, the nodal displacements of the joint panel can be calculated and the joint deformation modes will then be obtained from the nodal displacements as outlined below.

For the joint panel configuration shown in Figure 3.9, let the initial lengths of the potentiometers be B_0 (bottom), T_0 (top), N_0 (north), S_0 (south) and D_0 (diagonal). The instrumentation lengths in the deformed mode are defined as in Eq. 3.3 – 3.7 using the measured changes in lengths.

$$B = B_0 + \Delta B = d + \Delta B \tag{3.3}$$

$$T = T_0 + \Delta T = d + \Delta T \tag{3.4}$$

$$N = N_0 + \Delta N = h + \Delta N \tag{3.5}$$

$$S = S_0 + \Delta S = h + \Delta S \tag{3.6}$$

$$D = D_0 + \Delta D = \sqrt{d^2 + h^2} + \Delta D \tag{3.7}$$

By establishing the geometry of the joint from Eqs. 3.8 – 3.11 and constraining $u_8 = 0$, the remaining nodal displacements are calculated using Eqs. 3.12 – 3.18 with respect to the reference node 3 (i.e., $u_5 = u_6 = 0$).

$$\theta_1 = \cos^{-1}\left(\frac{B^2 + S^2 - D^2}{2BS}\right) \tag{3.8}$$

$$\theta_2 = \cos^{-1}\left(\frac{B^2 + D^2 - S^2}{2BD}\right) \tag{3.9}$$

(a) Joint panel nodal displacements

(b) Mode 1 - pure shear

(c) Mode 2 - extension in x direction

(d) Mode 3 - extension in y direction

(e) Mode 4 - curvature about x axis

(f) Mode 5 - curvature about y axis
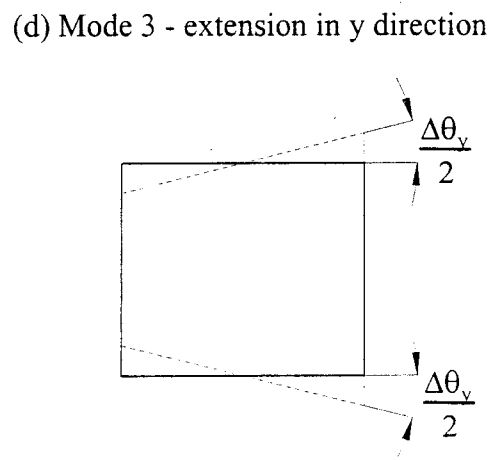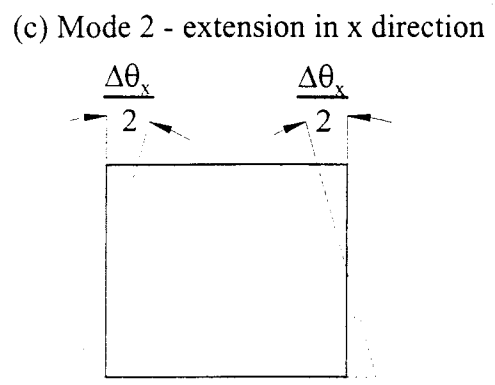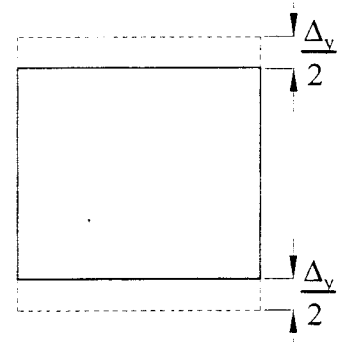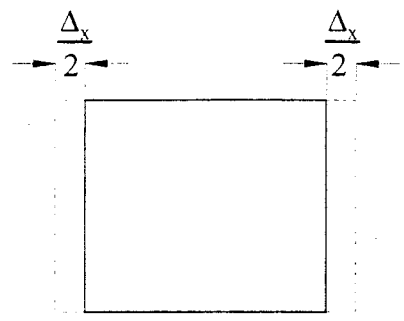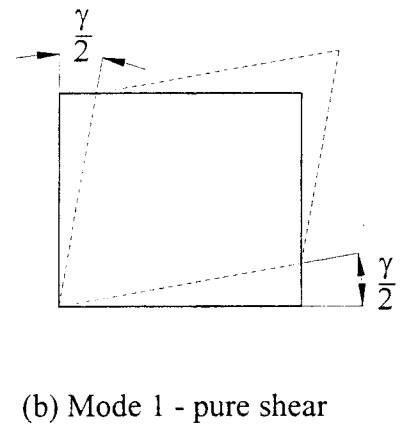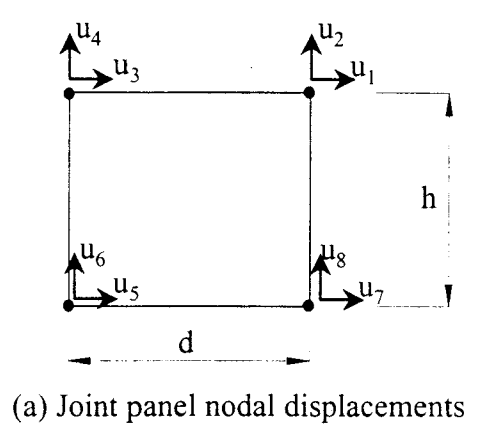
Figure 3.8 Independent joint panel deformation modes.

(a) Original geometry   (b) Deformed geometry
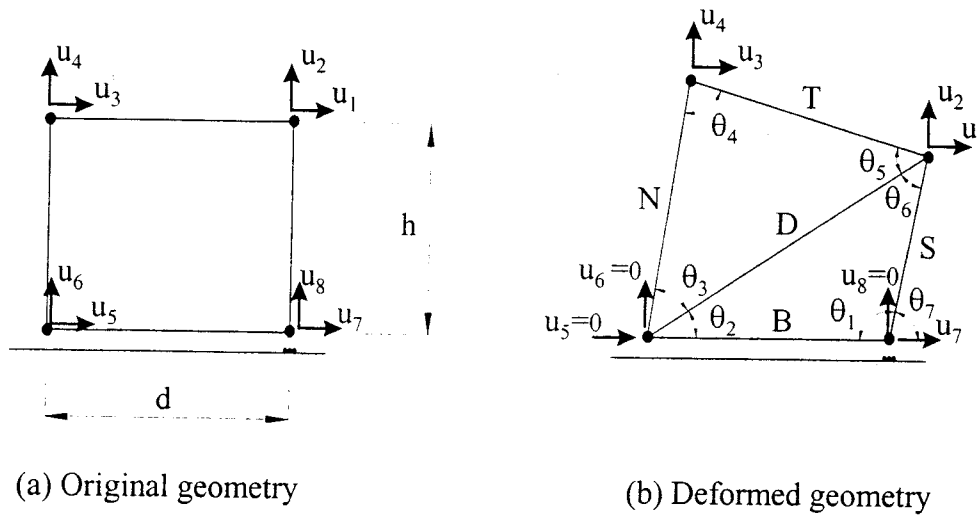
Figure 3.9 Joint panel deformation.

$$\theta_3 = \cos^{-1}\left(\frac{N^2 + D^2 - T^2}{2ND}\right) \tag{3.10}$$

$$\theta_7 = \pi - \theta_1 \tag{3.11}$$

$$u_1 = S\cos\theta_7 \tag{3.12}$$

$$u_2 = S\sin\theta_7 - h \tag{3.13}$$

$$u_3 = N\cos(\theta_2 + \theta_3) \tag{3.14}$$

$$u_4 = N\sin(\theta_2 + \theta_3) \tag{3.15}$$

$$u_5 = 0 \tag{3.16}$$

$$u_6 = 0 \tag{3.17}$$

$$u_7 = B - d = \Delta B \tag{3.18}$$

From nodal displacements of the joint panel, each joint deformation mode is obtained from Eq. 3.19.

$$\begin{Bmatrix} \gamma \\ \Delta\theta_x \\ \Delta\theta_y \\ \Delta_x \\ \Delta_y \end{Bmatrix} = \begin{bmatrix} \dfrac{1}{2h} & \dfrac{1}{2d} & \dfrac{1}{2h} & -\dfrac{1}{2d} & -\dfrac{1}{2h} & -\dfrac{1}{2d} & -\dfrac{1}{2h} & \dfrac{1}{2d} \\ -\dfrac{1}{h} & 0 & \dfrac{1}{h} & 0 & -\dfrac{1}{h} & 0 & \dfrac{1}{h} & 0 \\ 0 & \dfrac{1}{d} & 0 & -\dfrac{1}{d} & 0 & \dfrac{1}{d} & 0 & -\dfrac{1}{d} \\ -\dfrac{1}{2} & 0 & \dfrac{1}{2} & 0 & -\dfrac{1}{2} & 0 & \dfrac{1}{2} & 0 \\ 0 & \dfrac{1}{2} & 0 & -\dfrac{1}{2} & 0 & \dfrac{1}{2} & 0 & -\dfrac{1}{2} \end{bmatrix} \begin{Bmatrix} u_1 \\ u_2 \\ u_3 \\ u_4 \\ u_5 \\ u_6 \\ u_7 \\ u_8 \end{Bmatrix} \qquad (3.19)$$

The constraint $u_5 = u_6 = u_8 = 0$ does not introduce any error in the joint deformation components when calculated from Eq. 3.19, but it implies that the rigid body modes (one rotation and two translations) of the joint are zero.

3.3.1 Strain Gauges – Wall Direction Testing

Critical strain gauges in the wall direction of testing were located on the confinement reinforcement within 10 in. from the wall-to-foundation interface, on the first pair of U-shaped flexural plates from the base of walls and on the Dywidag unbonded prestressing bars. Strain gauges were also placed on the X-plates and topping reinforcement, which, respectively, connected the double tees and hollow-core floor panels to the seismic frames. Locations of the confinement reinforcement gauges are depicted in Figure 3.10a while details of the gauges in the UFP connectors are shown in Figure 3.10b. The strain gauges on the Dywidag bars were located at two levels; closer to the base of walls and at the horizontal joint between the wall panels. A summary of strain gauges relevant to the wall direction of testing is presented in Table 3.2.

3.3.2 External Devices – Wall Direction Testing

External instrumentation in the wall direction of testing consisted of displacement transducers, rotation devices and curvature cells. A summary of the general location and reference points of the displacement transducers is given in Table 3.3. At each floor level, two transducers located at 8 ft. apart in alignment with the actuator centerline were used as the control displacement devices for the tests. These transducers recorded the lateral movement of the building with respect to the steel frame of the test laboratory. After

considering several different options, the steel frame was chosen as the external reference frame for the wall direction of testing. It was found from monitoring the movement at regular intervals that the steel frame experienced a lateral displacement of up to 0.12 in. due to changes in ambient temperature. The thermal effects were severe in the mornings and reduced to below 0.02 in. by early afternoon. As a result, the tests were generally conducted from 2.00 p.m. onwards until the early morning hours of the following day. All significant pseudodynamic tests were delayed until 7.00 p.m. in order to maintain the lateral movement of the reference frame to within 0.01 in. during the course of each test.

(a) Transverse reinforcement   (b) UFP connector
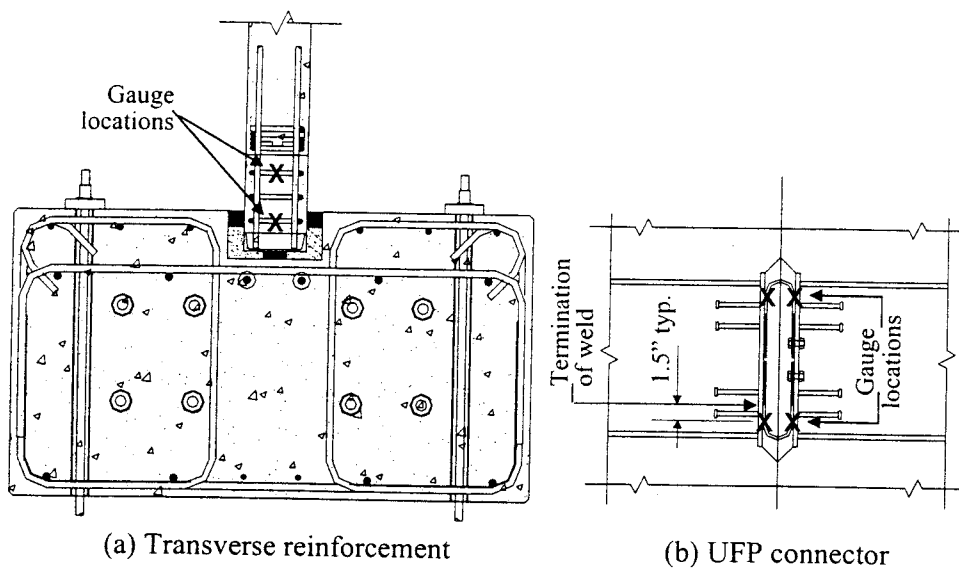
Figure 3.10 Confinement and UFP connector gauges in the wall system.

Table 3.2 Locations of strain gauges used in the wall direction of testing.

Location	To monitor	No. of gauges
Base of wall panel	Confinement strain	8
Wall strap	Tension demand on the straps	2
Prestressing bars in walls	Tensile strain	6
UFP connector	Strain in the flexural plates	4
Base of gravity column	Strain in the anchor bolt	2
X- plate connector	Force transfer from floor to seismic frame	5
Reinforcement in topping	Force transfer from floor to seismic frame	5
Flat bar connector	Force transfer between floor panels	3

41

Table 3.3 Locations of displacement transducers used in the wall direction of testing.

Device mounted to	Measured with respect to	Direction	Floor level	No. of devices
Floor panels	External reference frame	Horizontal	1 to 5	10[a]
Wall system	External reference frame	Horizontal	1 to 5	5
Wall panel	Wall Panel	Horizontal	0, 2.5	2
Wall panel	Wall panel	Vertical	0, 2.5, 5	4
Wall panel	Double-tee	Vertical	1 to 3	4
Wall panel	Hollow-core panel	Vertical	4	1
Base of walls	Foundation	Vertical	0	6
Base of columns	Foundation	Horizontal	0	5 pairs
Gravity beams	Columns	Horizontal	1, 4	16
Double-tee	Seismic frame	Horizontal	1 to 3	9
Double-tee	Double-tee	Horizontal	3	1
Hollow-core panel	Gravity frame	Horizontal	4, 5	3
Hollow-core panel	Gravity frame	Vertical	5	1
Hollow-core panel	Seismic frame	Horizontal	5	2
Hollow-core panel	Hollow-core panel	Horizontal	4, 5	10
Floor panels	Strong wall	Horizontal	3,5	4[b]
Reaction tower	External reference frame	Horizontal	Top	2
Reaction tower	External reference frame	Vertical	Base	3

[a]Used for controlling the wall direction tests, [b]Measured torsional displacement of the building

In addition, a displacement transducer per floor in the form of string potentiometer was used to measure the lateral displacement of the wall system with respect to the reference frame. These devices were mounted to the wall typically about 6 in. above the top of each floor. As indicated in Table 3.3, several transducers were also employed to monitor the relative movements between various precast elements.

The test building was equipped with four rotation devices in the wall direction of testing. Two of these devices were mounted on the steel channels connecting the wall system to the interior column of the TCY frame (i.e., column C7 in Figure 1.3) at floor levels 4 and 5. The remaining two devices were attached to a gravity column (i.e., C4) and a seismic exterior column (i.e., C1) at 12 in. below the bottom surface of the hollow-core panel at the fifth floor.

As noted in Table 3.3, the bases of five columns, including the two gravity columns, were instrumented with curvature cells. In the two gravity frames, 16 displacement transducers cells were also placed at the beam ends to monitor opening and closing of the gap between the gravity beams and various columns at floor levels 1 and 4.

3.3.3 Strain Gauges – Frame Direction Testing

The majority of gauges in the frame direction of testing were located within eight beam-to-column joints; one exterior and one interior joint from each of the four ductile frame connection types were chosen. As detailed in Table 1.1, the hybrid and TCY gap connections were located in the first three floors, and the pretensioned and TCY connections were used in the upper two floors. Consequently, all of the strain gauges were placed in the joints formed by Columns C1, C2, C3 and C4 at the first and fourth floor levels, where the maximum joint shear demand was expected to develop for the different joint types. Typical joint gauge locations are shown in Figure 3.11.

Strain gauge measurements in the frame direction were also taken on the starter bars at the base of six columns as detailed in Figure 3.12, on several beam longitudinal reinforcing bars close to the joint interface, and on the beam prestressing reinforcement. The gauges placed on the connecting elements of the floor systems in the wall direction of testing (see Table 3.2) were also monitored in the frame direction tests.

3.3.4 External Devices – Frame Direction Testing

The 15 ft. deep strong reaction wall of the test laboratory, to which the actuators were mounted (see Figure 3.5), was used as the reference system for recording the absolute lateral displacements of the test building at each floor level. The control displacement transducers used target points on the center of the inner face of the interior seismic columns at 2.5 in. above the top of the floor. In addition, a string potentiometer at each floor level was added part way through the frame direction testing (from IT2 test onwards, see Table 4.3) to measure the lateral displacement of the interior seismic column of the TCY frame (i.e., Column C7). These potentiometers used the unbonded precast loading tower (see Figure 3.2) as the reference system and monitored displacements at the center of outer face of the joints at all floor levels.

43
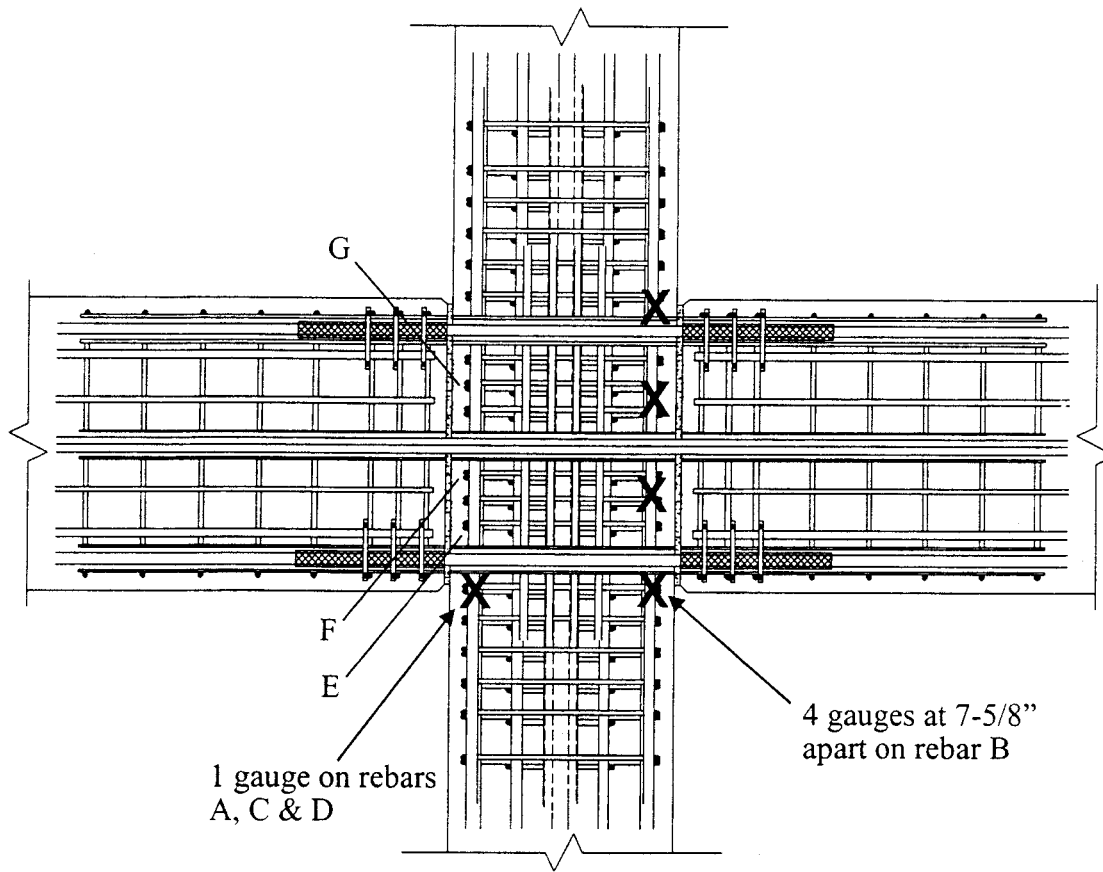
(a) Elevation
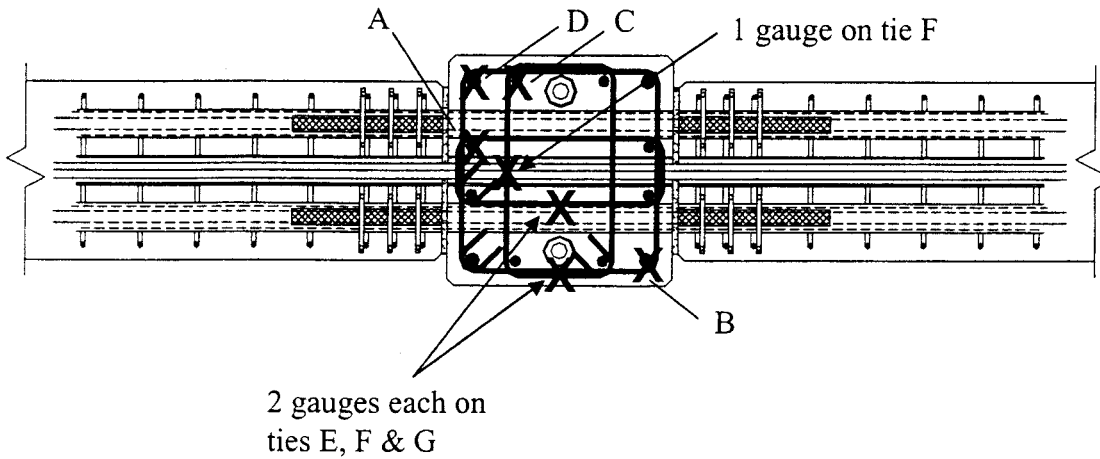
(b) Plan

Figure 3.11 Strain gauge locations in a hybrid interior frame connection.

Outer faces of all eight strain gauged beam-to-column joints were mounted with joint panel devices. Two additional joint panel devices were attached to the outer faces of

the two interior joints at the fifth floor level. Several curvature cells were placed at the beam and column ends adjacent to the joint panel devices as shown in Figures 3.7. The change in beam length between the two exterior columns was also monitored with a string potentiometer at each floor level in the two seismic frames.
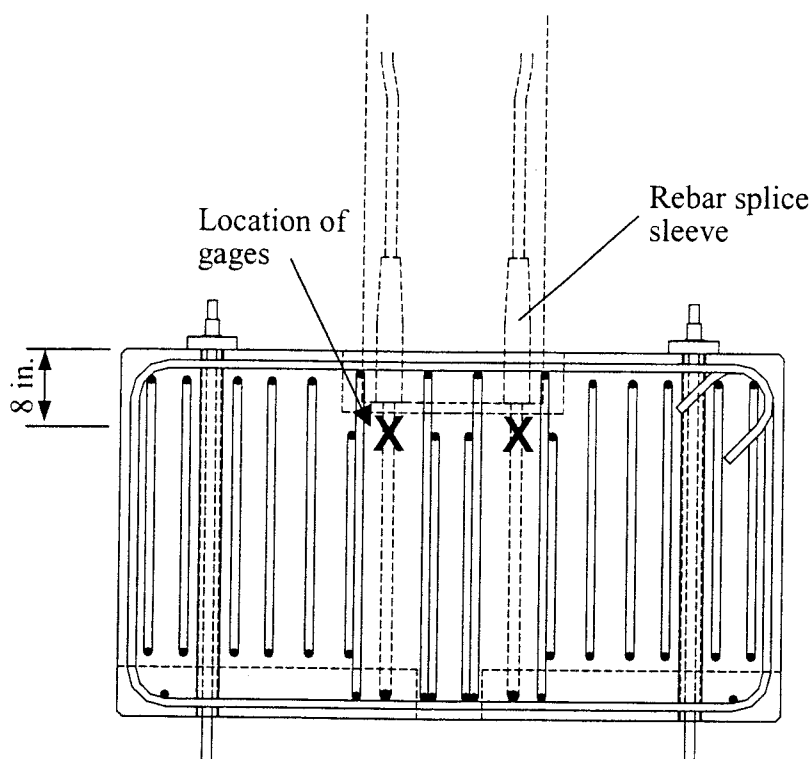
Figure 3.12 Location of strain gauges on the column starter bars.

Some of the external instrumentation used in the wall direction of testing was relocated prior to the frame direction of testing while several instruments specific to the wall direction of testing were disconnected. The curvature cells at the column bases were repositioned to measure deformation in the plane of loading. The displacement transducers placed at the third and fifth floor to monitor the torsional displacements in the wall direction were also relocated for convenience. All four rotation devices used in the wall direction were transferred to the inner faces of seismic columns C1, C2, C6 and C7. In C1 and C2, the device was positioned at 18 in. below the bottom surface of the hollow-core panel at the fifth floor, while, in C6 and C7, the rotation devices were mounted to the center of column stubs extending above the fifth floor.

The displacement transducers, which were used for the control of the test, string potentiometers, curvature cells and displacement transducers recorded the in-plane response of the wall system were disconnected. Recording of the displacement transducers that were mounted to the gravity beams was also discontinued in the frame direction of testing. The remaining displacement transducers, which were used primarily to monitor relative movements of the precast floor panels in the wall direction testing (see Table 3.3), were monitored during testing in the frame direction.

CHAPTER 4

SEISMIC TEST DETAILS

Testing of the PRESSS building was conducted parallel to the jointed wall system and seismic frame direction independently. As detailed in Section 3.1.1, the lateral load resistance of the seismic columns was minimized when the building was subjected to seismic testing in the wall direction. The frame direction of testing was then followed, which included the lateral load resistance of the walls due to out-of-plane bending. The contribution of the wall resistance in the out-of-plane direction was relatively small. Furthermore, this arrangement provided an opportunity to examine the interaction between the jointed wall system and the floors during the frame direction testing. In the wall and frame directions, seismic testing was conducted following application of axial loads in the columns to simulate appropriate gravity effects as discussed in Chapter 3.

Seismic testing in each direction consisted of three types of tests, namely the stiffness measurement test, the pseudodynamic test, and the inverse triangular load test. Description and objectives of each test type are given below. A significant portion of the seismic testing of the PRESSS building in each direction was performed using the pseudodynamic testing procedure for a series of preselected earthquake motions. Following a description of the different testing procedures, the selection process of suitable input acceleration time histories and the test sequences are presented in this chapter.

A test control program for conducting the three different tests mentioned above was developed previously for testing of a five-story masonry building by Igarashi [23]. A significant effort was made in the development of this program to improve efficiency of testing while minimizing propagation of error by implementing appropriate numerical algorithms. The original source code of the program had been developed in VMS FORTRAN, which was rewritten in Visual C^{++} to be compatible with the new control system that was used in the PRESSS building test. A special feature of this test control program is that it is capable of conducting tests on rigid structures such as a masonry building using a soft coupling technique (see Section 4.2). Due to relatively high flexibility of the precast building, this feature was not activated during the PRESSS building test.

4.1 Stiffness Measurement Test

The stiffness measurement test is a quasi-static loading test through which the stiffness matrix of a structural model can be formulated. Updating of the stiffness matrix following an increase in the intensity of the lateral seismic loading is often useful for

a) determining the appropriate integration time step when explicit schemes are used in solving the equation of motion in the pseudodynamic testing procedure,

b) improving convergence of implicit integration schemes in the pseudodynamic testing procedure,

c) monitoring overall structural damage using stiffness as a damage indicator, and

d) examining implications of the force-based and the direct-displacement based design methods.

The stiffness measurement test can be conducted under force or displacement control. The control program included three different methods, namely the conventional stiffness measurement test, flexibility measurement test and modal stiffness measurement test [23]. The first and the third methods facilitate tests under displacement control while the second method uses a force control algorithm. For the PRESSS building test, the flexibility method was predominantly used and the procedure is discussed below. The description of the other two test methods may be found in Reference [23].

In the flexibility method, the test building is subjected to **n** load sets independently, where **n** is the degrees of freedom assumed for the building model. In the first load set, the actuators mounted at the first floor level apply equal forces to the building while maintaining the remaining actuators at zero loads. In the subsequent sets, the loads are applied at Floors 2 through **n** in the same manner (see Figure 4.1). An appropriate load for each set should be chosen such that the corresponding displacement vector **x** can be measured with sufficient accuracy, and (b) the resulting response of the building will be in the elastic range. A displacement matrix X_{nxn} is then formed by combining all **x** vectors such that the columns 1 through **n** in **X** represent the measured **x** for load sets from **1** to **n**. The flexibility matrix of the structure is, therefore, **X** and the stiffness matrix is established from Eq. 4.1.

$$K_{nxn} = X_{nxn}^{-1}$$

(4.1)
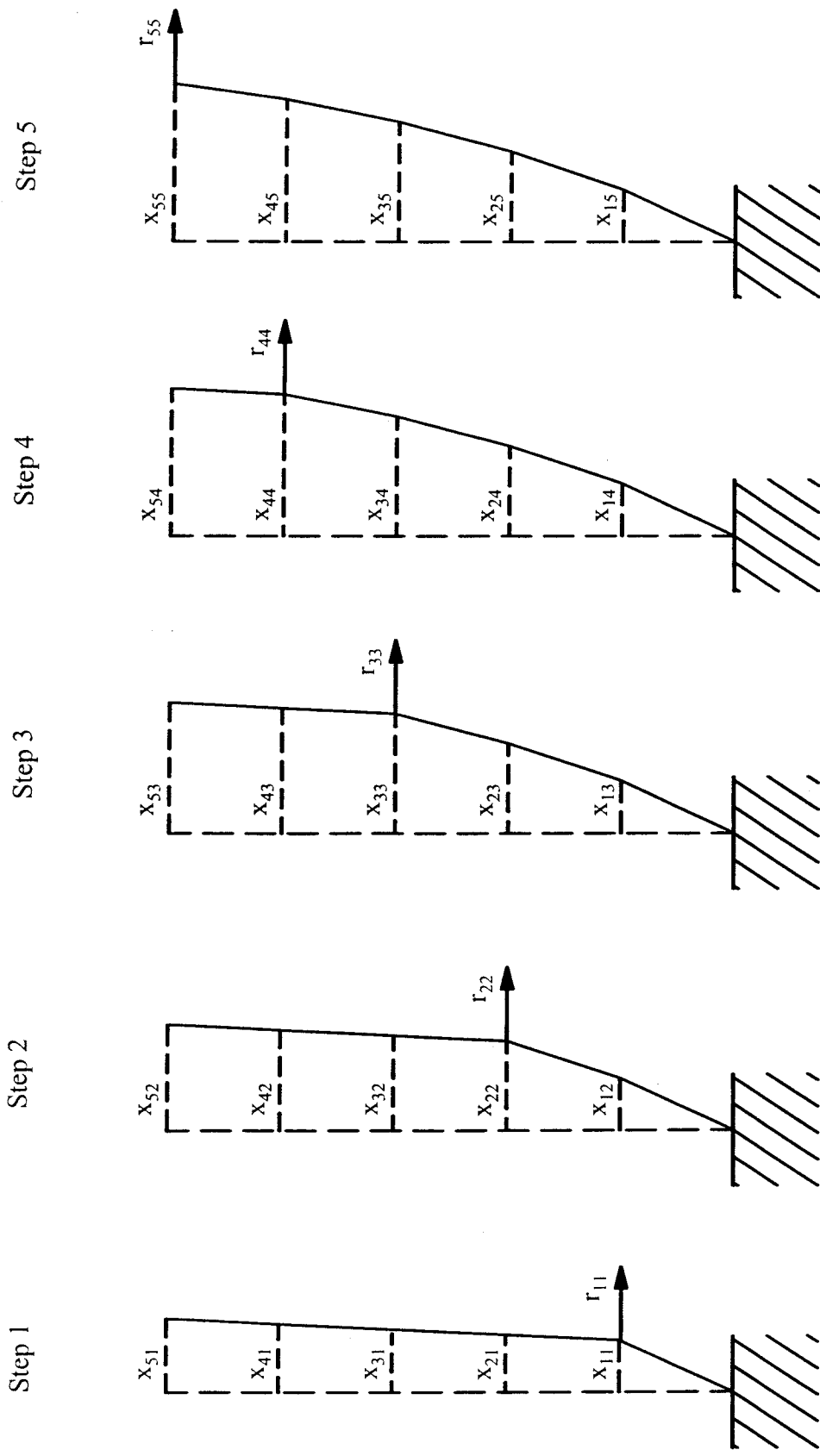
Figure 4.1 Flexibility measurement test demonstrated for a structure with 5 transnational DOF.

49

In the PRESSS test, lateral loads in each set were applied in the push and pull directions and the average measured displacements of the floors in the two directions were used to formulate X_{nxn}. In order to ensure that the stiffness matrix would be symmetric, K was refined as follows:

$$K = \frac{1}{2}\left[K_{nxn} + K_{nxn}^T\right] \tag{4.2}$$

where K^T is the transpose of K established from Eq. 4.1.

4.2   Pseudodynamic Test Procedure

Real-time shake table seismic testing is not practically feasible on large structural models such as the PRESSS building, and the pseudodynamic technique provides an alternative method for evaluating the performance of these models under a given earthquake input record. In this method, the external dynamic load is applied to the structure quasi-statically through on-line controlled hydraulic actuators. Combining numerical computation and experimental measurements, the pseudodynamic test is carried out as illustrated in Figure 4.2. The numerical computation is performed on a computer model representing the test structure. By assigning n degrees of freedom (DOF), the dynamic equation of motion of the computer model can be expressed as

$$M\ddot{x}(t) + C\dot{x}(t) + r(t) = f(t) \tag{4.3}$$

where t is the time variable, M is the nxn mass matrix, C is the nxn damping matrix, x is the nx1 structural displacement vector, r is the nx1 restoring force vector, and $f(t)$ is the nx1 external force vector. For structural response in the linear range, $r(t)$ in Eq. 4.3 can be replaced with $Kx(t)$, where K is the nxn stiffness matrix as defined in Eq. 4.2.

By appropriately defining mass and damping matrices (i.e., M and C) for the computer model, the pseudo-dynamic test is conducted in the following manner:

Step 1: In addition to defining M and C matrices, assign initial conditions (i.e., $x(0)$ and $\dot{x}(0)$), and the external force vector $f(t)$.

Step 2: Set time step $i = 1$
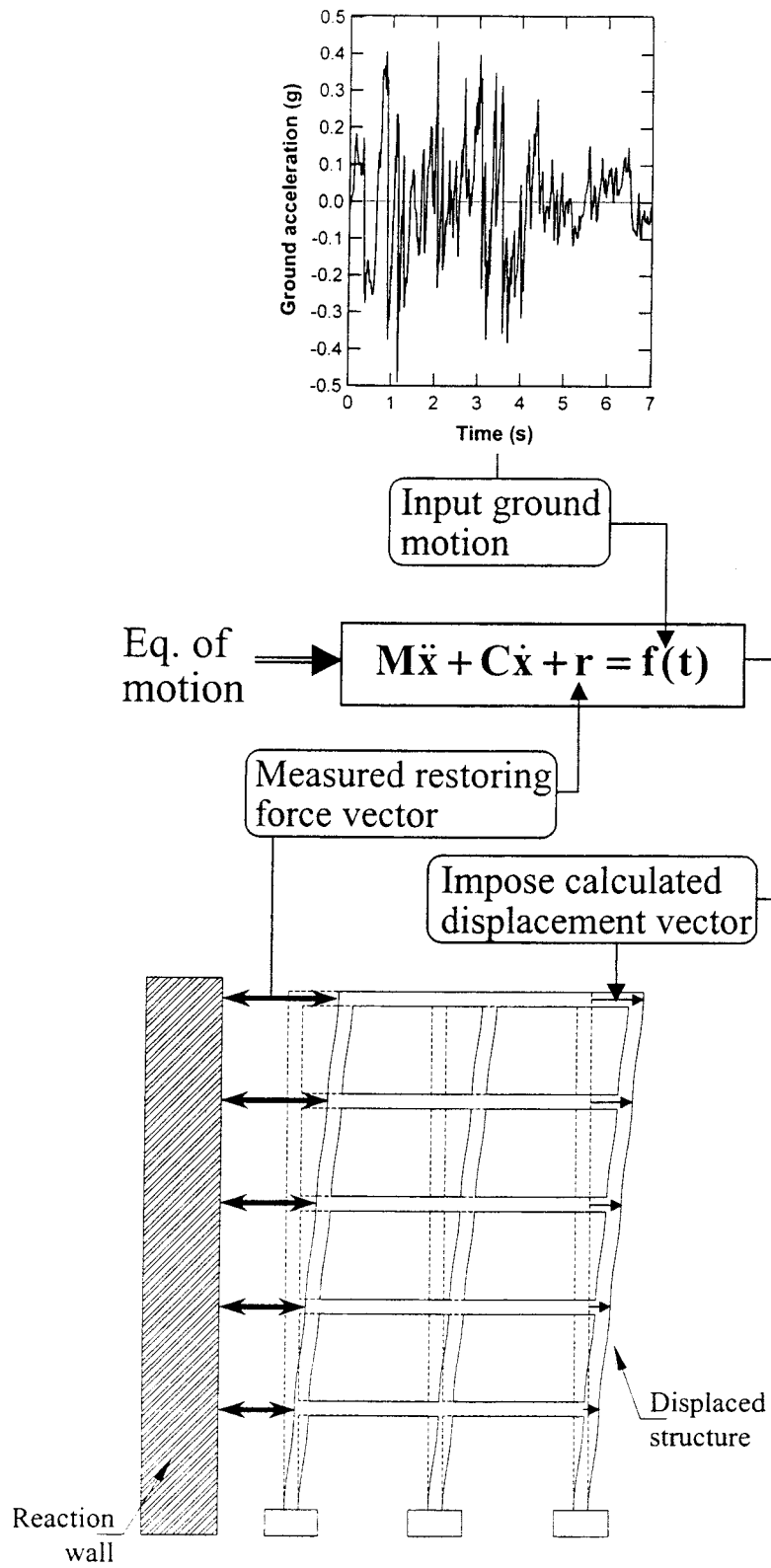
Figure 4.2 Pseudodynamic test concept.

Step 3: Using a suitable numerical integration scheme, solve Eq. 4.3 for **x(i)**

Step 4: Displace the test structure for computed **x(i)** and measure **r(i)**

Step 5: Set **i = i+1** and repeat steps 3 – 5.

Although the test steps outlined above appear to be straightforward, selecting a suitable integration scheme and controlling propagation of experimental error resulting from sources, such as the numerical integration, inaccurate displacement measurements and short fundamental period of the structure, are the keys to a successful pseudodynamic test. When dealing with pseudodynamic testing of the TCMAR five-story stiff masonry building, Igarashi [23,24] examined the propagation of experimental error in detail and developed a pseudodynamic testing algorithm suitable for stiff multi-degree-of freedom (MDOF) systems. This software included several improvements to then existed pseudodynamic testing procedures of stiff MDOF systems and several on-line strategies to minimize error propagation during testing. The critical issues addressed by Igarashi in developing the software can be summarized as follows:

- Use of the modified Hilber method for solving equation of motion.
- Displacement error resulting from the difference between *computed* and *measured* actuator displacements.
- Faster convergence of target displacements in each time step Δt.
- Controlling actuators connected to a test structure through soft coupling. Use of elastomeric pads parallel to the loading plane introduced the necessary soft coupling in the testing of the masonry building.
- DOF reduction technique to eliminate DOF corresponding to torsional rotation of the floors.
- Actuator displacement filtering – as part of error growth control, in a multiple layer actuator system, it is necessary to restrict the actuators from imposing displacements corresponding to higher modes.

The pseudodynamic testing software developed by Igarashi was used for testing the PRESSS building without incorporating any soft coupling between the actuators and the test structure. As noted previously, the original source code was translated from FORTRAN to Visual C++ such that the software would be compatible with a new hardware system. In addition, appropriate graphics user interface was created.

The PRESSS building modeled only one wall system at 60% scale. Hence, the weight associated with each floor of the test building was taken as

$$19,500 * \frac{1}{5} * \frac{1}{4} * 0.6^2 = 351 \text{ kips}$$

The corresponding seismic mass responsible for inducing inertia force at each floor level was assumed to be

$$351 * \frac{1}{386.4} = 0.9084 \text{ kips/in./s}^2$$

Hence, the mass matrix of the computer model in the wall direction was taken as

$$\mathbf{M} = \begin{bmatrix} 0.9084 & 0 & 0 & 0 & 0 \\ 0 & 0.9084 & 0 & 0 & 0 \\ 0 & 0 & 0.9084 & 0 & 0 \\ 0 & 0 & 0 & 0.9084 & 0 \\ 0 & 0 & 0 & 0 & 0.9084 \end{bmatrix} \quad (4.4)$$

Accounting for 50% reduction in the number of bays of the seismic frames in the test building, the mass matrix of the computer model for the frame direction tests was taken as

$$\mathbf{M} = \begin{bmatrix} 1.817 & 0 & 0 & 0 & 0 \\ 0 & 1.817 & 0 & 0 & 0 \\ 0 & 0 & 1.817 & 0 & 0 \\ 0 & 0 & 0 & 1.817 & 0 \\ 0 & 0 & 0 & 0 & 1.817 \end{bmatrix} \quad (4.5)$$

It was realized after completing the tests of the PRESSS building that the mass matrices, as presented above, are incorrect. The above calculation used gravitational force $g = 386.4 \text{ in/s}^2$. Since the length and time in the model building are scaled at 60%, the gravitational force should have been modified as

$$g = 386.4 * \frac{0.6}{0.6^2} = 644.0 \text{ in.} / \text{s}^2$$

The above g value provides seismic mass at each floor of 0.5450 kips/in/s² and 1.090 kips/in/s² for the wall and frame directions, respectively. These values are 40% less than those used in the actual tests.

Use of higher seismic mass implies that the PRESSS test building modeled larger prototype structures than those intended in Figures 1.1 and 1.2. The floor area of the buildings in these figures is 100x200 sq. ft. The seismic mass assumed in the tests represents prototype structures with a floor area of 129x258 sq. ft.

Good agreement between experimental and analytical results was obtained for the PRESSS building tests [20,25], both of which used identical mass matrices. Therefore, variation in responses due to the difference in mass values may be further investigated through analytical means. A limited investigation was conducted using the frame direction model presented by Pampanin et al. [20]. It was found that reducing seismic mass by 40% generally reduced the floor forces by about 15 – 25 percent in the frame direction. However, the peak floor force obtained during the design level earthquake was not altered due to the change in the mass values. No consistent observation could be made for the displacement histories obtained using the different mass matrices. However, the reduced mass resulted in smaller peak displacements for input records weaker than the design level event. For the design level earthquake, the peak displacement was 5% higher than that obtained with the mass matrix shown in Eq. 4.5.

The change in critical results due to the difference in mass is small because the reduced mass altered the natural period of the structure by only 23 percent. Also, in both cases, the building models responded with significant hysteresis actions. Therefore, main conclusions reached from the tests of the PRESSS building remain unchanged.

When pseudodynamic tests are performed in a quasi-static manner, the velocity dependent viscous damping is not activated in the test structure since the actual velocity of the structure during testing is almost zero. However, the viscous damping effect can be accounted for in a pseudodynamic test by appropriately defining damping matrix C in Eq. 4.3. Use of the same C matrix at different levels of testing may not be appropriate. For example, if stiffness-proportional damping is chosen for the test structure, then it follows

that different **C** matrices should be adopted for the elastic and inelastic responses. Also, use of large damping coefficients for higher unwanted modes was necessary during the PRESSS test to suppress the influence of these modes and improve efficiency of the testing procedure. Consequently, different **C** matrices were defined at different levels of pseudodynamic testing. Details of the various tests conducted on the PRESSS building in the wall and frame directions and the corresponding **C** matrices are reported in Section 4.5.

4.3   Inverse Triangular (IT) Test

In an inverse triangular test, the structural model is subjected to a displacement profile appropriate for exercising the test structure through its fundamental mode of response. The purpose of IT tests is twofold. In the design of structures using FBD or DDBD, member forces are determined by subjecting the structure to an inverse triangular load pattern, which primarily captures the effects of the first mode response. Such design models can be validated from experimental data of IT tests. In the DDBD procedure, the design base shear at the target drift is determined using an equivalent viscous damping for the entire structure (see Section 2.3). This critical design parameter, which was established through detailed analytical models [11,12], can be experimentally quantified from IT tests.

In IT tests, the appropriate displacement profile is determined for a specified top floor displacement using the current estimate of the stiffness matrix. This displacement profile is expected to develop a restoring force vector proportional to an inverse triangular pattern if the estimate of the stiffness matrix is accurate. More details including the convergence technique adopted in the IT tests may be found in References [23,24].

The PRESSS building was subjected to IT tests at different limit states in both directions of testing. The maximum absolute displacement of the top floor recorded in the previous pseudodynamic test was typically set as the target top floor displacement for the subsequent IT test. Details of the different levels of IT tests conducted on the PRESSS building in the wall and frame directions are reported in Section 4.5.

For tests IT4 and IT5 in the frame direction (see Table 4.3), the procedure outlined above could not be followed since an accurate estimate of **K** was not possible due to progressive damage occurred to the TCY frame. Consequently, these two IT tests

were performed for a target fifth floor displacement while ensuring an inverted triangular force distribution in each set of five actuators along the height of the building. This was achieved by placing the actuators connected to Floors 1 – 4 under force-control and slaving them with appropriate functions to the top floor actuators, which were taken to the target value under displacement control.

4.4   Selection of Earthquake Input Records

The reasons to adopt the EQ III level spectra proposed by PBE-SEAOC in the design of the PRESSS building was discussed in Section 2.4. Since the expected performance of buildings when subjected to the four levels of earthquakes identified by PBE-SEAOC (see Ref. 16) correlate well with the anticipated degree of protection in the four different limit states described in Section 2.2, it was desired to conduct the pseudodynamic test of the PRESSS building to earthquakes with intensities increasing from EQ I to EQ IV. The 5% damped acceleration response spectra corresponding to the four levels are shown in Figure 4.3 while the compatible displacement spectra can be found in Figure 2.5.
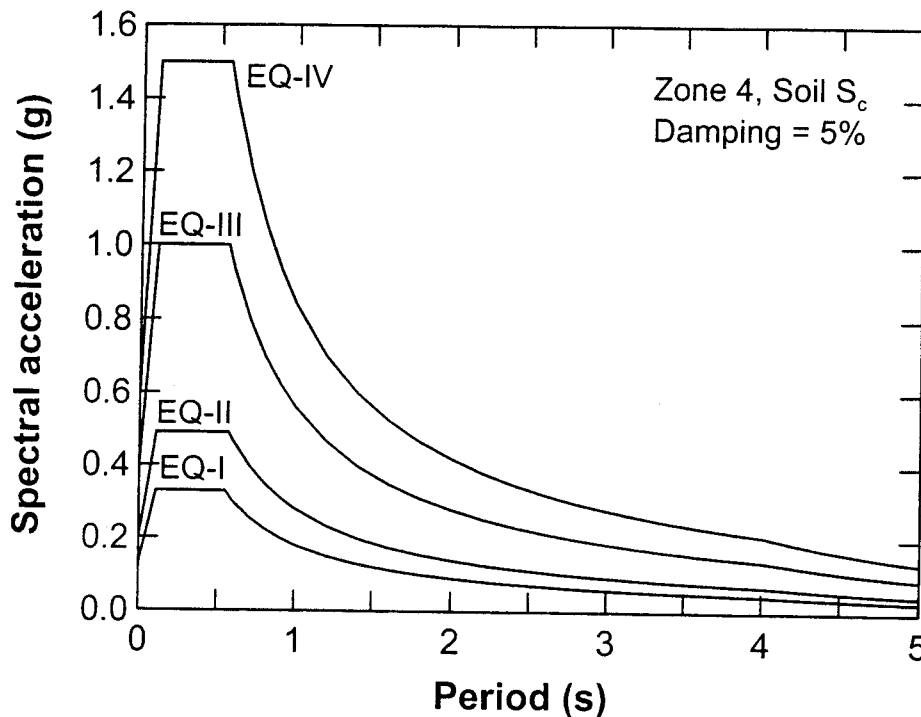
Figure 4.3 Acceleration response spectra for earthquake hazard from EQ-I to EQ-IV [16].

It was not feasible to compile a suite of acceleration time histories representative of the four levels using recorded ground motions from the past earthquakes. Instead of

56

employing synthetic records, appropriate input motions for pseudodynamic testing of the PRESSS building were established by modifying recorded earthquake motions on soil type S_c. This section describes the derivation of compatible input motions. Difficulties faced during testing of the building to EQ III and EQ IV level input motions and further modifications introduced to these records are discussed in Section 4.5.

Steps involved in deriving a spectrum compatible acceleration time history is described by establishing an EQ-III level input motion using the S00E component of the El Centro record obtained from the 1940 Imperial Valley earthquake. Pseudodynamic tests are time consuming and performing a test over one second of the earthquake record may require over 30 minutes depending on the stiffness of the test structure. As a result of this and due to the fact that pseudodynamic tests are accompanied by IT tests whose effect on the structure is as severe, if not more than the pseudodynamic tests, the duration of the input records was kept to a minimum value that would be sufficient to encompass the strong segment of the original earthquake record. Duration in the range of 4 – 9 seconds was used for input motions representing EQ I to EQ IV level earthquakes.

The duration of El Centro record is 53.7 s and a seven-second segment of this record containing the peak acceleration cycle was used in deriving the EQ-III level input motion for pseudodynamic testing. The starting time of all segments, except for EQ-I motion, was decided such that the first peak of each segment is the first peak in the record exceeding 0.1g ground acceleration. For EQ-I level input motion, the same criterion was used with the first peak exceeding 0.05g.

In Figure 4.4, the 5% damped acceleration response spectra obtained for 53.7 s and 7 s duration of the El Centro record are compared with the corresponding EQ-III spectrum. Close agreement obtained for the two El Centro spectra confirms that the strong portion of the original record is included in the 7 s segment extracted for the test simulation. This segment was then modified such that it provided an acceleration spectrum comparable to the EQ-III spectrum. In Figure 4.4, it can be seen that the spectrum of the modified motion satisfactorily matches the EQ-III spectrum. The necessary modification to the earthquake segment was performed using program SHAPE [26], in which the changes were made iteratively by multiplying Fourier amplitudes of the original motion by spectral ratios established between target acceleration response spectrum and spectrum of the input motion. The original and modified segments of the El Centro records are shown in Figure 4.5.
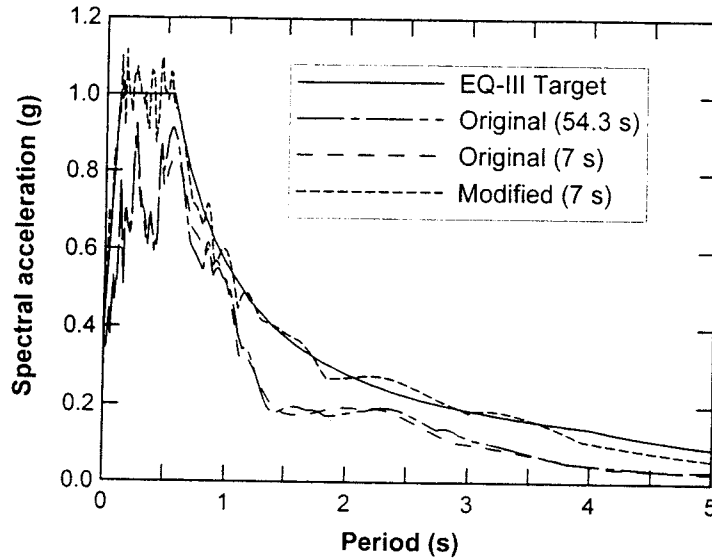
Figure 4.4 EQ-III spectrum and 5% damped El Centro acceleration response spectra.

(a) Original segment

(b) Modified segment
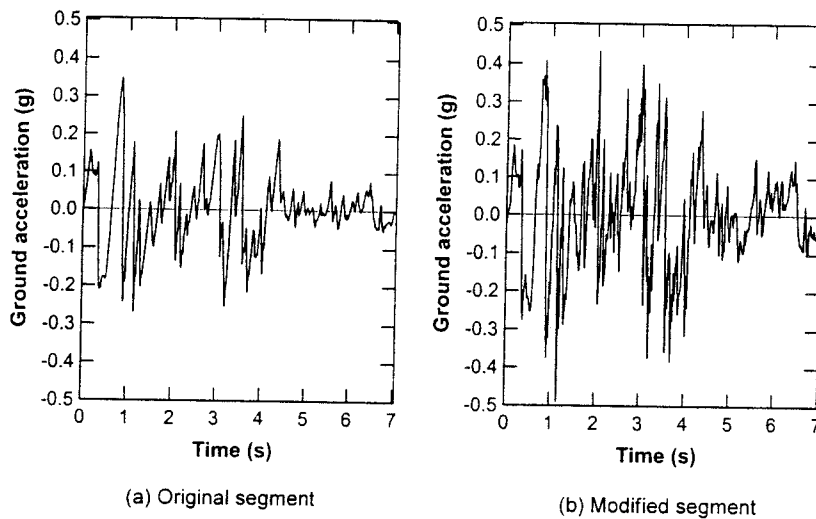
Figure 4.5 Seven-second segment of the El Centro record.

Four other input motions derived for possible application in the pseudodynamic test of the PRESSS building are shown in Figure 4.6 and descriptions of the corresponding original records are given in Table 4.1. Two input motions were simulated at EQ-IV level using original records from a Californian and an overseas earthquake. It is noted that in all modified motions, some high frequency content uncharacteristic of natural records is apparent, which elevated the peak ground acceleration (PGA) of the modified records by as much as 50% higher than the target PGA. Low-pass filtering of these records would eliminate the high frequency content and reduce the PGA closer to the target values. However, such filtering was considered unnecessary because the response of the test

58

building was not expected to be sensitive to the high frequency content responsible for elevating the PGA.
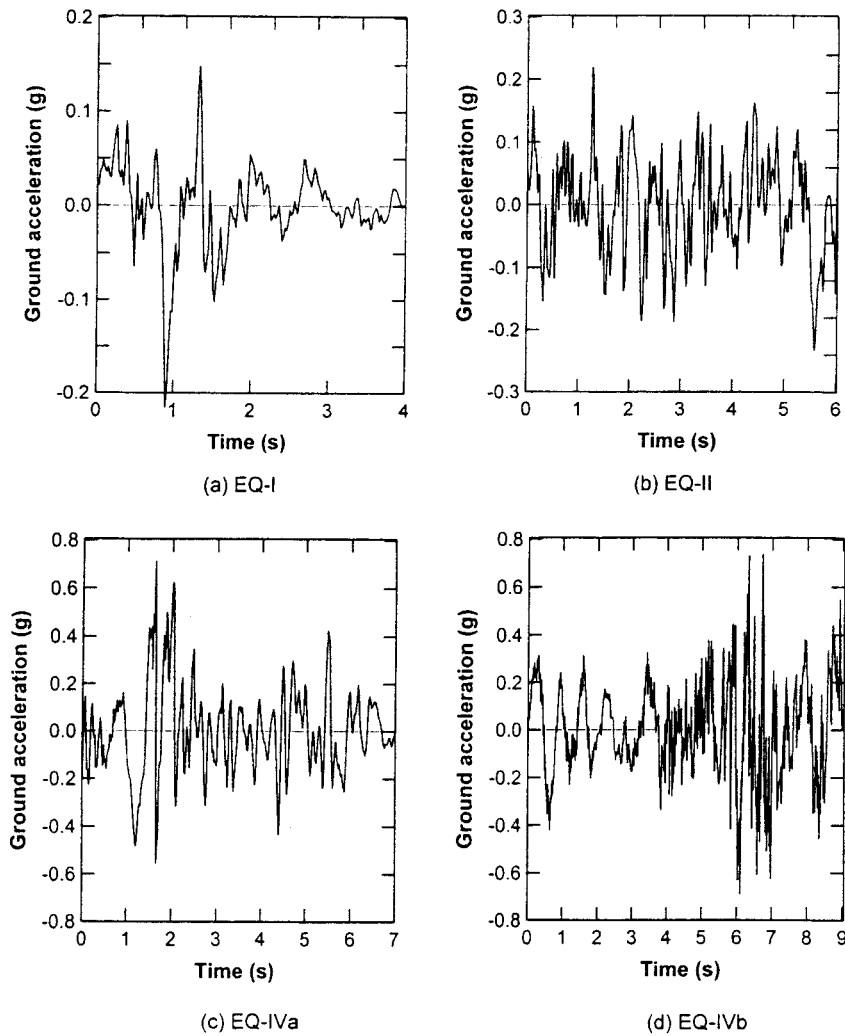
Figure 4.6 Four other input motions derived for the PRESSS building test.

Table 4.1 Details of earthquake records used to derive the test input motions.

EQ Level	Earthquake	Magnitude	Record	PGA
I	1974 Hollister	$M_L = 5.2$	Gilroy Array #1 (S67W)	0.14g
II	1971 San Fernando	$M_W = 6.6$	Hollywood Storage (N90E)	0.21g
III	1940 Imperial Valley	$M_W = 6.9$	El Centro (S00E)	0.35g
IVa	1993 Northridge	$M_W = 6.7$	Sylmar (N00E)	0.84g
IVb	1978 Tabas	$M_W = 7.4$	Tabas (N16W)	0.94g

The design of the PRESSS building was performed using the displacement spectra, and thus it is of interest to compare the displacement spectra of the above records with the corresponding design spectra. In Figures 4.7 and 4.8, the 5% and 20% displacement spectra are compared for all four levels of earthquakes. At 5% damping, good agreement between the spectral displacement ordinates of the input records and target values is seen for up to about 3 – 4 s except for EQ-IV based on the Sylmar record. At EQ-III and EQ-IV intensity levels, the comparison at 20% damping is more critical. While the spectral ordinates of the input motion are in satisfactory agreement with the target values for the EQ-III motion, the input motions at EQ-IV level, in particular the record that based on the ground motion at Sylmar, contained spectral displacements significantly greater than the target values. Since the input motions were established by matching acceleration spectra at 5% damping, some discrepancies between the spectral displacements of the input motions and target spectral ordinates were expected at higher damping.

Furthermore, a satisfactory match between the acceleration spectral ordinates at 5% damping was not possible for the input motion based on the Sylmar record. Unlike that demonstrated for EQ-III motion in Figure 4.4, a significant peak at a period of about 0.35 s and spectral ordinates over a broad period band of 1 –3 s could not be reduced to match the target spectrum satisfactorily using SHAPE. Unsatisfactory matching of the spectral acceleration at 0.35 s and over the broad period band explains why spectral displacements of the corresponding input motion did not match the target displacement spectra in Figures 4.7d and 4.8d. Pending further investigation, it was concluded that the simulated input motion based on the Sylmar record contained more energy than that expected from a record matching the EQ-IV spectrum and might not be appropriate for testing of the PRESSS building.

The simulated input motions shown in Figures 4.5 and 4.6 should be applied to the structure at the prototype scale. Due to 60% scale adopted for the PRESSS building, an appropriate scaling of the input records was necessary. By selecting a scale factor of 0.6 for length and time, the acceleration and time step of the input motions for the PRESSS test were modified by multipliers 1/0.6 and 0.6, respectively.

In order to simulate free vibration of the test building following the response to an earthquake, the scaled input records were padded with zero acceleration ordinates for an additional 1.5 – 5.75 s of duration. The pseudodynamic tests, which typically included

the free vibration phase, were typically terminated when the change in the absolute displacement amplitude was close to zero at each floor level.
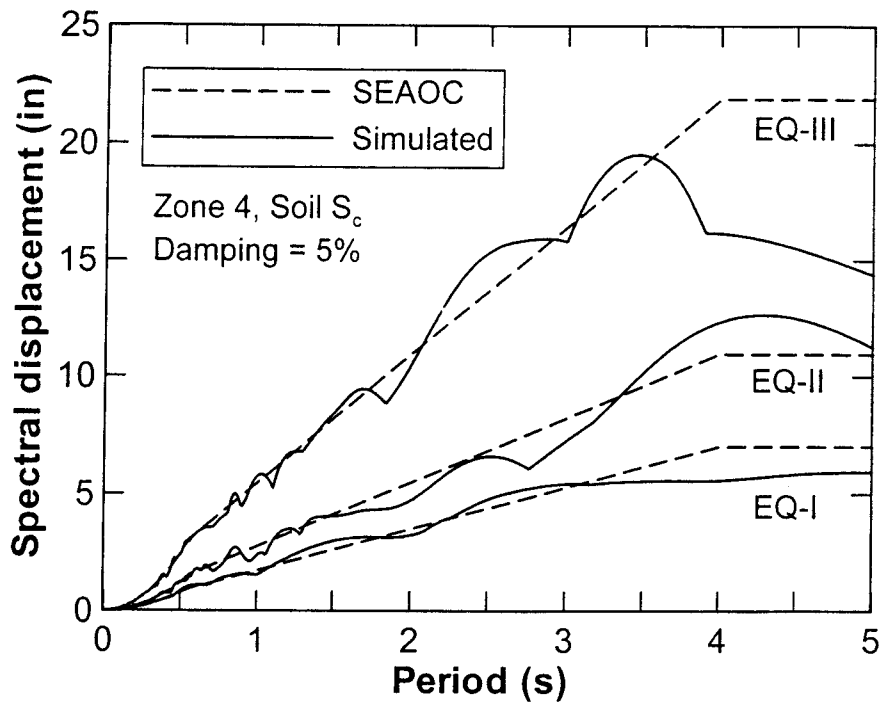
(a) EQ-I, II and III
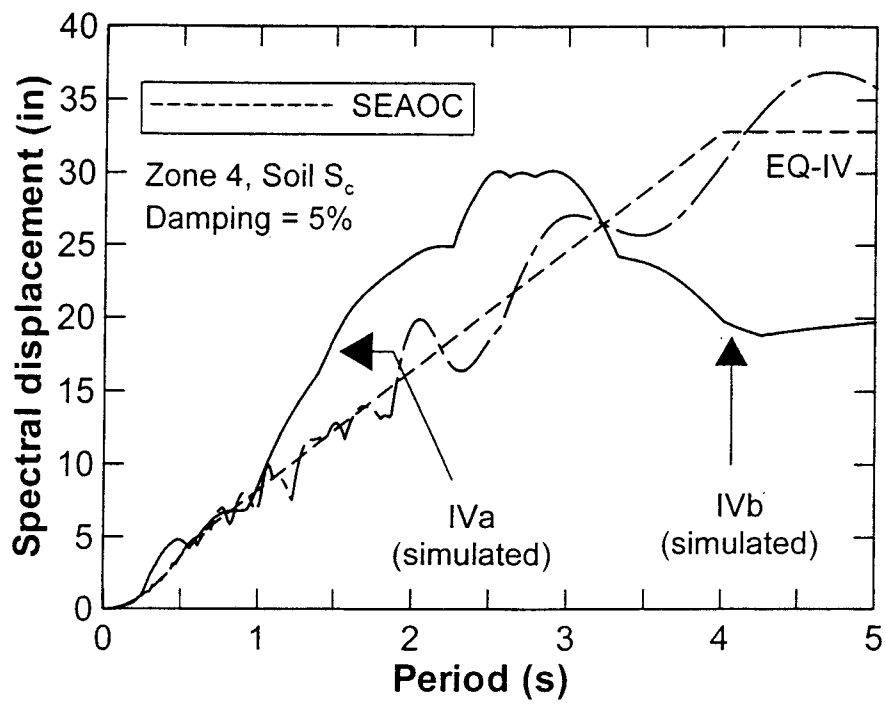
(b) EQ-IV

Figure 4.7 Comparison of displacement spectra for the simulated input motions.

61
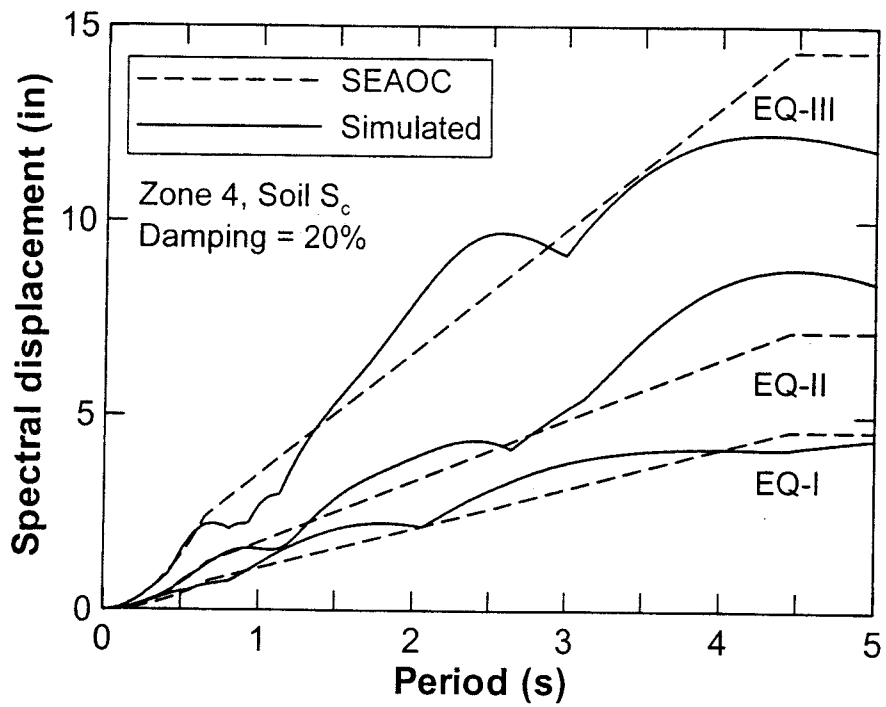
(a) EQ-I, II and III
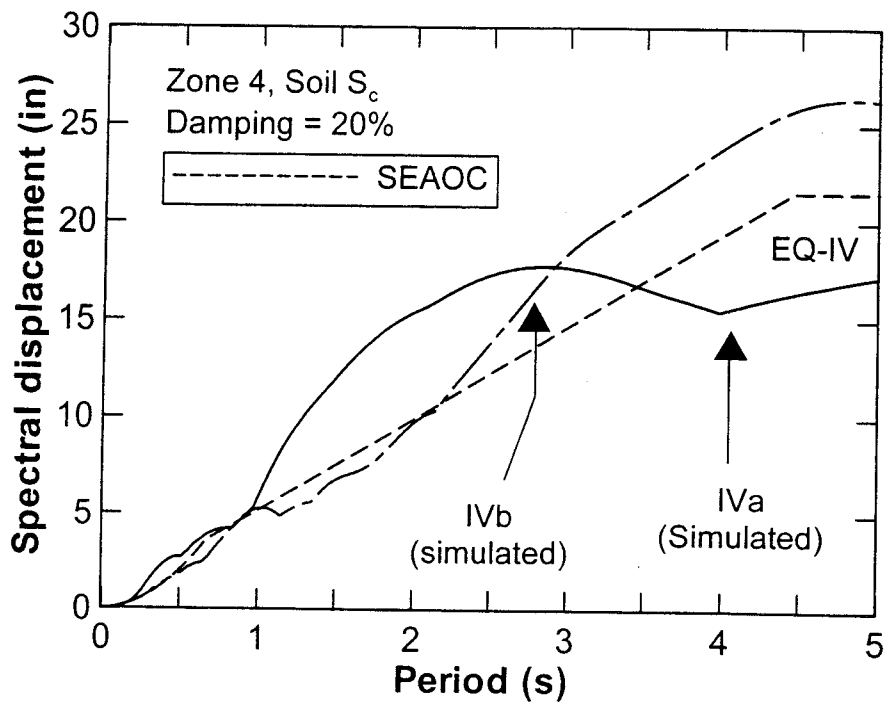
(b) EQ-IV

Figure 4.8 Comparison of displacement spectra for the simulated input motions.

62

4.5 Test Sequence and Further Modifications to Input Records

As mentioned previously, the PRESSS building was first tested in the wall direction and then tested parallel to the seismic frames. Seismic testing procedure adopted in the two directions was similar. The stiffness matrix of the building in the uncracked state was first formulated through a stiffness measurement test. Several low amplitude pseudodynamic tests, often using sine waves as input motions, and inverse triangular tests were performed as diagnostic tests. Subsequently, the building was subjected to two pseudodynamic tests with 0.25EQ-I and 0.50EQ-I as the input motions. This was followed by a sequence of tests consisting of a pseudodynamic test, an inverse triangular test, and a stiffness measurement test. This sequence was repeated several times with intensity of the input motion for the pseudodynamic test increasing from that representative of EQ-I to EQ-IV. At each level of the input motion, the inverse triangular test having a minimum of one cycle with full reversal was performed such that the resulting maximum positive and negative roof drifts were equal to the maximum recorded drift in the preceding pseudodynamic test. A summary of all significant tests conducted in the wall and frame directions are given in Table 4.2 and 4.3, respectively.

As can be noted in Tables 4.2 and 4.3, the stiffness measurement tests were omitted when the damage to the building during the pseudodynamic and IT tests was minimal. Pseudodynamic tests were sometimes repeated and the corresponding input motions were modified by a multiplier of –1 where appropriate. When a test had to be aborted due to various reasons, the actuator loads were brought to zero forces and, if necessary, the displacement of floors were brought to near zero values by subjecting the building to an IT test of a smaller magnitude.

Pseudodynamic tests in the two directions were conducted successfully for EQ-II, EQ-I and lower levels of input motions. It was apparent in these tests that the response of the PRESSS building was significantly influenced by higher mode effects. This observation was also supported by analytical models which were used to predict the response prior to conducting the tests [20,25]. In the design of the test building, allowance for higher mode effects greater than the code recommended values was made. However, the observation of tests up to EQ-II level input motion confirmed that the higher mode effects required much larger floor forces at all five levels. The analytical models also predicted that the floor forces at lower levels would reach near the actuator

force capacity and demand yielding of the steel fixtures connecting the actuators to the building floors when subjected to the EQ-III input motion.

Table 4.2 List of significant tests conducted in the wall direction.

Test No.	Test Description	Max. Lateral Displacement at the 5th Floor (in)	Max. Base Shear (kips)
025	0.25*EQ-I	0.200	89.66
032	0.50*EQ-I	0.417	142.10
033	1.0*EQ-I(1)	1.211	315.14
034	IT-I(1)	1.247	186.42
036	IT-I(2)	1.248	172.99
038	1.0*EQ-I(2)	1.752	285.23
039	-1.0*EQ-I	1.635	295.52
040	1.0*EQ-II	3.020	295.73
041	IT-II	3.084	221.59
046	-1.0*EQ-II	2.905	301.51
051	1.0*EQ-III(modified)	8.343	323.51
052	IT-III(1)	8.337	301.59
054	IT-III(2)	8.340	279.20
055	-1.5*EQ-III(modified)	11.531	465.87

Table 4.3 List of significant tests conducted in the frame direction.

Test No.	Test Description	Max. Lateral Displacement at the 5th Floor (in)	Max. Base Shear (kips)
107	0.25*EQ-I	0.567	120.70
108	0.50*EQ-I	1.173	201.22
110	1.0*EQ-I	2.626	340.87
111	IT-I	2.633	256.41
112	1.0*EQ-II	6.845	333.15
113	IT-II	7.069	341.81
116	1.0*EQ-III(modified)	9.992	353.54
117	IT-III	10.310	350.30
119	IT-IV	12.371	347.06
120	IT-V	19.901	369.87

procedure when solving the equation of motion. This was also a consideration when selecting the damping values for the tests.
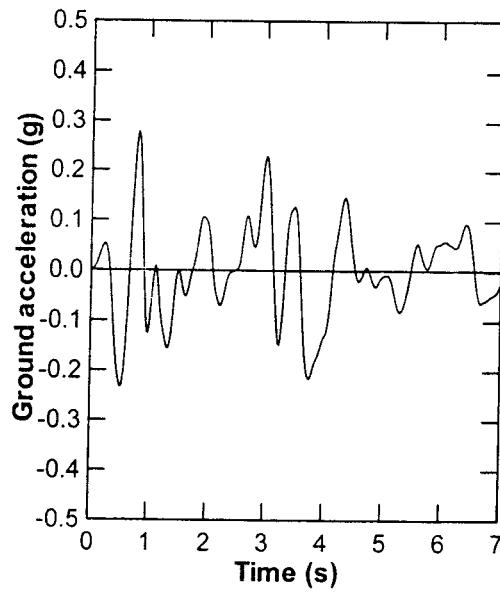
(a) Input motion
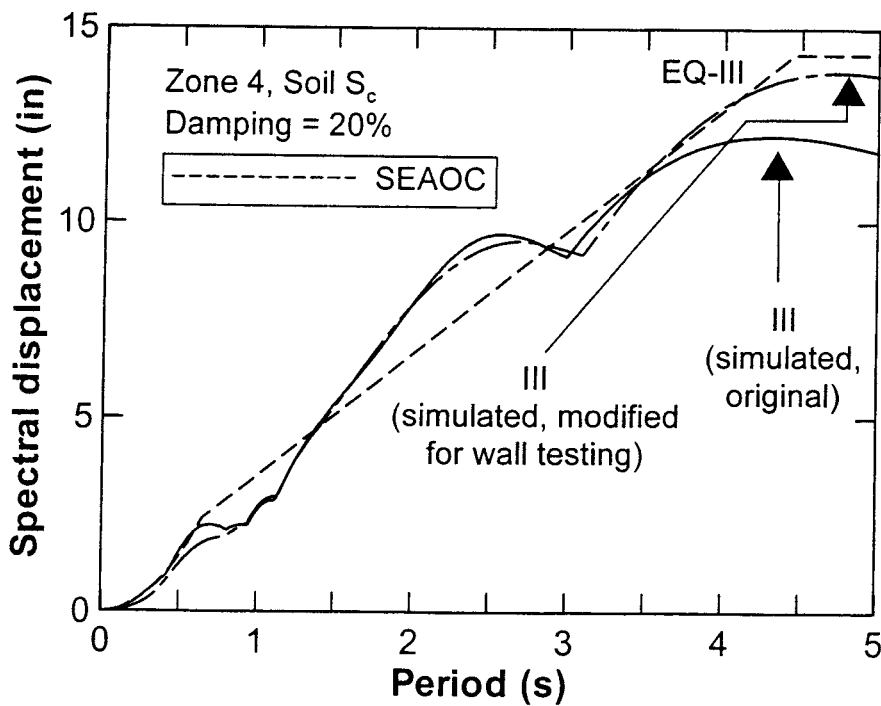
(b) Displacement spectra

Figure 4.9 The modified EQ-III input motion used in the wall direction of testing.
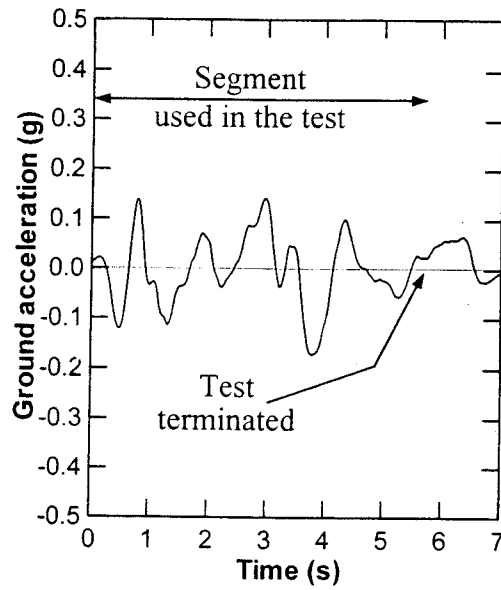
(a) Input motion
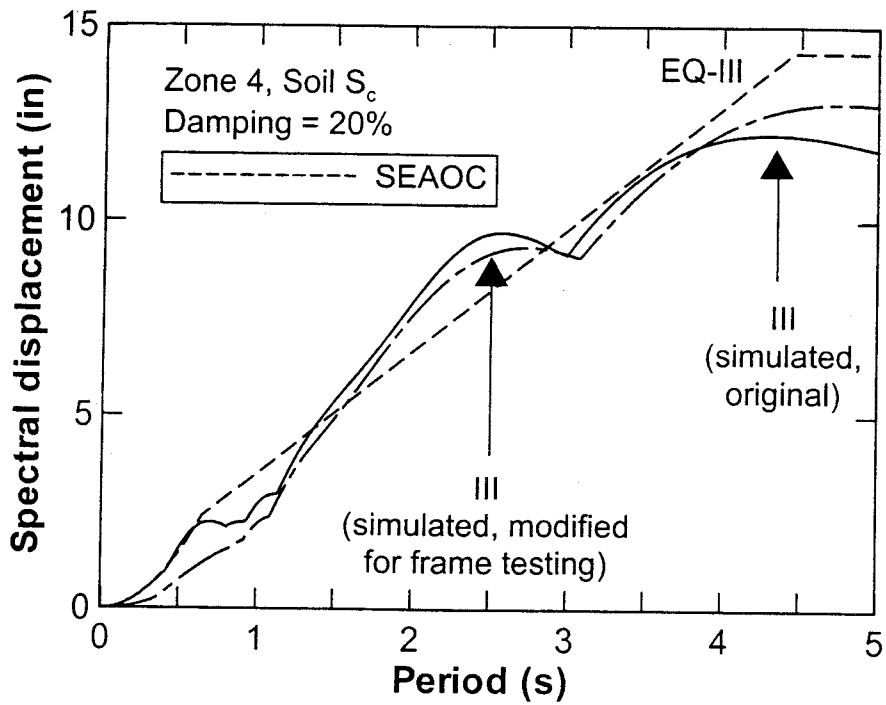
(b) Displacement spectra

Figure 4.10 The modified EQ-III input motion used in the frame direction of testing.

The damping matrix, C, for each test was defined as $[\Phi^{-1}]^{T}[c][\Phi^{-1}]$, where $[\Phi]$ represents the eigen vectors (or mode shapes) and $[c]$ is a diagonal matrix with each diagonal term representing $2\zeta(\lambda)^{\frac{1}{2}}$. In the diagonal term, ζ is the damping ratio and λ is the eigen value of the corresponding mode. At different levels of testing, ζ values were preassigned for the five modes associated with the five DOF. Since the λ value is defined using the elastic rather than the tangent stiffness of the structural system, it was felt appropriate to reduce the viscous damping ratio for the first mode as the intensity of the input motion was increased. This modification provides a more appropriate C matrix for the response of the structure in the nonlinear range.

In the wall direction of testing, ζ = [5%, 5%, 10%, 70%, 70%] was assigned for the five modes up to EQ-II level of testing. For greater intensity motions (i.e., for EQ-III and beyond), the damping ratio of the first mode was reduced to 2.5% while no changes were made to damping ratios of the higher modes. As can be seen from the definition of ζ, the fourth and fifth modes were heavily damped out in the wall direction of testing as it was found from the diagnostic testing of the PRESSS building that these modes would not be reliably accounted for in the laboratory tests.

In the frame direction of testing, ζ = [5%, 5%, 10%, 70%, 70%] was used at the initial stages of testing. Since actuator displacements did not always converge to the target displacements within the permissible limits, no further changes to the damping ratios were considered in the frame directions of testing.

CHAPTER 5

SUMMARY AND
CONCLUDING REMARKS

This is the third of 10 volumes of reports produced on the large-scale seismic testing of the PRESSS five-story precast concrete building. Overall design verification, instrumentation and test design procedures are discussed in this volume. Significant portions of the test in the wall and frame directions were pseudodynamic, in which the building was subjected to earthquake input motions whose intensities were progressively increased from that representing a frequent event to that comparable to a maximum considered earthquake in Zone 4.

In parallel with the pseudodynamic testing, behavior of the PRESSS building was predicted prior to performing tests at each intensity level to examine any potential problems in conducting the pseudodynamic tests. The analytical models and the predicted response of the building, which was in satisfactory agreement with the observed behavior, are reported in Volumes 3-4 [20] and 3-5 [25] for the wall and frame directions, respectively. In addition, detailed and independent analyses of the response of the PRESSS building were performed by Lehigh University, which will be reported separately in Volume 3-7. A summary of the experimental results may be found in Refs. [27,28]

5.1 Design Verification

The PRESSS building was designed using the direct-displacement based procedure. It was found that the overall base shear in the wall and frame directions were almost identical to that calculated by the design team. There was no further check done for the jointed wall system. For the seismic frames, the beam end design moments were compared with the corresponding moment strengths established at a frame drift of 2%. The reinforcement details reported by the design team were used for calculating the various beam strengths. It was found that the design moment was less than the moment strength at the ends of all beams. The beams in the prestressed frame had an average overstrength of 18% whereas the average overstrength of the TCY frame beams was 27%. A larger average overstrength should be expected for the TCY frame due to the fact

that the TCY gap system inherently has a greater negative moment resistance than the positive moment resistance. No modifications to the reinforcement details were suggested.

5.2   Instrumentation

The PRESSS building was extensively instrumented in the two directions of testing with a primary objective of characterizing the overall performance of the building. Several instruments were also employed to record the relative movements between various precast members.

The rotation and uplift of the wall panels at the base, and strains in the unbonded prestressing bars, UFP connector and several connecting elements between the floor panels and seismic frames were recorded in the wall direction of testing. While continuing with recording of strains in the connecting elements, beam and column end rotations, joint panel deformation and tension demand on the beam-to-column joint reinforcement were also monitored at an interior and an exterior joint representing the four precast ductile frame systems in the frame direction of testing.

5.3   Seismic Testing

Seismic testing in each direction consisted of stiffness measurement, pseudodynamic and inverse triangular tests. Appropriate numerical algorithms to successfully execute the different test types were previously developed for a five-story masonry building [23,24]. Using these three types of tests, the PRESSS building was sufficiently exercised to seismic effects at different intensity levels in two directions: parallel to the wall system first and then parallel to the seismic frames. A significant portion of testing in each direction was performed using the pseudodynamic testing procedure for a series of earthquake input motions. These input motions, which represented four intensity levels from EQ-I to EQ-IV as defined by PBE-SEOAC in Ref. [16], were established by modifying records from past earthquakes.

Pseudodynamic testing at intensity level EQ-III and above could not be carried out due to significant influence of higher mode effects. The forces required at lower floors almost reached or exceeded the capacity of the elements connecting the floor panels together and floor panels to the perimeter frame despite allowing for greater

higher mode effects in the design of the PRESSS building than code recommendations. The demand that the higher mode effects caused also exceeded the capacity of the steel fixtures connecting the actuators to the floor panels. Subsequently, modifications to the input motions were necessary to subdue the high frequency content. A discrepancy in the used and intended mass values was found after completion of the test. Analysis of the frame direction response revealed that the floor forces during testing could have been enhanced by about 15 – 25% due to the discrepancy in the mass. However, the peak displacements of the test building at the design level earthquake remained the same.

Analytical predictions of the PRESSS building in the frame and wall directions indicated that the input motions corresponding to EQ-IV would impose significantly higher drifts than about 3% expected at this intensity of earthquake motion. Pending further investigation of the EQ-IV level input records, 1.5xEQ-III was used as an appropriate input motion for EQ-IV level testing. Pseudodynamic testing at this intensity level was conducted only in the wall direction. Due to some limited damage that occurred to the TCY frame starting from EQ-II level of testing, pseudodynamic testing at EQ-IV was not performed in the frame direction. However, the seismic frames were tested under inverse triangular load distribution up to an interstory drift of 4.5%.

REFERENCES

1. Priestley, M. J. N., "Overview of PRESSS Research Program," *PCI Journal*, Vol. 36, No. 4, July-August 1991, pp. 50-57.

2. Nakaki, S. D., and Englekirk, R. E., "PRESSS Industry Seismic Workshops: Concept Development," *PCI Journal*, Vol. 36, No. 5, September-October 1991, pp. 54-61.

3. Stanton, J. F., Hawkins, N. M., and Hicks, T. R., "PRESSS Project 1:3 Connection Classification and Evaluation," *PCI Journal*, Vol. 36, No. 5, September-October 1991, pp. 62-71.

4. Priestley M. J. N., *Report of the 5th U.S. PRESSS Coordinating Meeting*, PRESSS Report 95/1, University of California at San Diego, La Jolla, CA, November 1995.

5. Priestley, M. J. N., "The PRESSS Program Current Status and Proposed Plans for Phase III", *PCI Journal* Vol. 41, No. 2 March-April 1996, pp. 22-40.

6. Nakaki, S. D., Stanton, J. F., and Sritharan, S., "An Overview of the PRESSS Five-Story Precast Test Building," *PCI Journal*, Vol. 44, No. 2, March-April 1999, pp. 26–39.

7. Stone, W. C., Cheok, G. S., and Stanton, J. F., " Performance of Hybrid Moment-Resisting Precast Beam-Column Concrete Connections," *ACI Journal*, Vol. 92, No. 2, March-April 1995, pp. 229-249.

8. Palmieri, L., French, C., Sagan, E. I., and Kreger, M. E., *Ductile Connections for Precast Concrete Frame Systems*, Proceedings of the Mete Sozen Symposium, ACI Special Publication SP–162, American Concrete Institute, Detroit, August 1996, pp. 313–335.

9. Sritharan, S. and S. D. Nakaki, "Construction Details and Material Properties", PRESSS Phase 3: The Five-Story Precast Test Building (Vol. 3-2), Department of Civil and Construction Engineering, Iowa State University, Ames, (in preparation).

10. Schultz, A. E., Tadros, M. K., Huo, X., and Magana, R., *Seismic Resistance of Vertical Joints in Precast Shear Wall Panels*, Proceedings of the FIP 1994 XII Congress, Washington, D. C., May-June 1994, 17 pp.

11. Collins, R. H., "Design of a Precast Concrete Building for Seismic Loading", MS Thesis, Department of Civil and Environmental Engineering, University of Washington, Seattle, 1999.

12. Galusha III, J. G., "Precast, Post-Tensioned Concrete Walls Designed to Rock", MS Thesis, Department of Civil and Environmental Engineering, University of Washington, Seattle, 1999.

13. Loeding, S., Kowalsky, M., and M. J. N. Priestley, "Direct Dispalcement-Based Design of Reinforced Concrete Building Frames", Report No. SSRP – 98/08, Structural Systems Research Project, University of California, San Diego, January 1998.

14. Priestley, M. J. N., "Displacement Based Approaches to Rational Limit States Design of New Structures," Presented at the Eleventh European Conference on Earthquake Engineering, Paris, September 1998.

15. Uniform building Code, International Conference of Building Officials, Whittier, CA, 1994.

16. PBE Ad-Hoc Committee of Structural Engineers Association of California, APPENDIX I - Tentative Guidelines for Performance Based Seismic Engineering Guidelines, SEAOC Blue Book, 1999.

17. Building Seismic Safety Council, NEHRP Recommended Provisions for Seismic Regulations for New Buildings and Other Structures, National Earthquake Hazard Reduction Program, Washington, D. C., 1997.

18. Uniform building Code, International Conference of Building Officials, Whittier, CA, 1997.

19. Eurocode 8, Design Provisions for earthquake resistance of structures, ENV 1998, Comité Europeen de Normalization, Brüssels, 1994.

20. Pampanin, S., M. J. N. Priestley and S. Sritharan, "Frame Direction Response", PRESSS Phase 3: The Five-Story Precast Test Building (Vol. 3-4), Report No. SSRP – 2000/08, Department of Structural Engineering, University of California at San Diego, California, November 2000.

21. Carr, A. J., RUAUMOKO – Inelastic Dynamic Analysis Program, University of Canterbury, 2000.

22. Priestley M. J. N., Seible, F. and Benzoni, G., "Seismic Performance of Circular Columns with Low Longitudinal Steel Ratios", Structural Systems Research, Report No. SSRP 94/08, University of California at San Diego, California, 1994.

23. Igarashi, A., "On-Line Computer Controlled Testing of Stiff Multi-Degree-of-Freedom Structural Systems under Simulated Seismic Loads", Doctoral Dissertation, Division of Structural Engineering, University of California, San Diego, 1994.

24. Igarashi, A., F. Seible, G. Hegemier, and M. J. N. Priestley, "The U.S.-TCCMAR Full-Scale Five-Story Masonry Research Building Test: Part III – Seismic Load Simulation", Report No. SSRP – 94/03, Structural Systems Research Project, University of California, San Diego, January 1994.

25. Conley, J., M. J. N. Priestley, S. Sritharan, "Wall Direction Response", PRESSS Phase 3: The Five-Story Precast Test Building (Vol. 3-5), Report No. SSRP – 99/19, Department of Structural Engineering, University of California at San Diego, California, July 2002.

26. Earth Mechanics, Computer Program: SHAPE, Fountain Valley, California, 1998.

27. Priestley, M. J. N, S. Sritharan, J. R. Conley, and S. Pampanin, S., "Preliminary Results and Conclusions from the PRESSS Five-Story Precast Concrete Test Building", *PCI Journal*, Vol. 44, No. 6, 1999, pp. 42-67.

28. Sritharan, S., "Performance of Four Jointed Precast Frame Systems under Simulated Seismic Loading", Proceedings of the Seventh U. S. National Conference on Earthquake Engineering, Paper No. 480, Boston, Massachusetts, July 2002.